PHYSICAL REVIEW B VOLUME 16, NUMBER 10 15 NOVEMBER 1977

Many-body processes in x-ray photoemission line shapes from Li, Na, Mg, and Al metals

P. H. Citrin and G. K. Wertheim
Bell Laboratories, Murray Hill, New Jersey 07974

Y. Baer
Laboratorium für Festkörperphysik, Eidgenössische Technische Hochschule, CH-8049, Zürich, Switzerland
(Received 23 May 1977)

X-ray photoemission from all the accessible core levels in Li, Na, Mg, and Al have been measured with Al $K\alpha$ radiation from metal films evaporated in ultrahigh vacuum, and the asymmetric line shapes of the core-level spectra were analyzed in terms of the Doniach-Šunjić (DS) function. Observed lifetimes were compared with theoretical calculations and showed generally good agreement for the $1s$ and $2p$ levels of Na, Mg, and Al but poor agreement for the $2s$ levels. The Li $1s$ lifetime was found to be considerably longer than predicted from simple atomic calculations, but was in good accord with a more recent many-body calculation. Singularity indices were determined from data extending to within half the Fermi energy from the main peak. The range of validity of the DS function and the possible line shape interferences from other sources were carefully examined, showing that the electron-hole pairs measured in the asymmetic tails are an intrinsic property of the bulk-metal spectrum and that the DS function gives an excellent representation of the data over a wide range of energies. The magnitude and trend of the singularity indices for Na, Mg, and Al were interpreted in terms of the partial screening charges associated with the hole-state atom and were found to compare favorably with several recent calculations. Detailed investigation of temperature-dependent phonon broadening magnitudes and zero-point and phonon cutoff energies were carried out for Li, indicating that a recently proposed interference effect may be responsible for the anomalously large line-shape broadening in that metal. At present, however, no theory adequately accounts for the observed Li $1s$ linewidth. For Na, Mg, and Al, on the other head, enhanced broadening effects were not observed and recent calculations of phonons broadening agreed well with our measurements. The Li $1s$ binding energy was observed to be temperature dependent, and its magnitude and trend were explained by a combination of anharmonic lattice expansion and the heretofore unappreciated temperature dependence of the electronic screening energy. The surface plasmon energy of clean Li was found to be in marked disagreement with that predicted from the empirical bulk plasmon energy and simple free-electron theory and still remains to be explained. The validity of the sudden approximation used in the interpretation of the electron-hole pair and phonon spectra observed in this work is also discussed.

I. INTRODUCTION

When a core electron is suddenly removed from an atom in a metal, the response of the remaining many electrons and nuclei gives rise to phenomena which are quite different from those observed in a system made up of a single atom with one electron, like atomic hydrogen, or even one with many electrons, like argon. Although understandably attractive and of great utility, simple one-electron models cannot give insight into such phenomena in many-body systems. Add to this the question regarding the meaning of "suddenly removed," i.e., sudden versus adiabatic, and the coexistence of intrinsic and extrinsic effects on the energy of the photoelectron, and it becomes clear that the interpretation of many-body phenomena in many-body systems must be firmly established before they can be expected to gain general acceptance.

This work reports on x-ray photoemission (XPS) line shapes of core electrons in the metals Li, Na, Mg, and Al, and interprets the observed spectra in terms of a many-body response. We shall demonstrate that our observations are indeed intrinsic and are consistent with interpretations assuming sudden electron removal. Our ultimate goal is to obtain a description of the many-body response in terms which help to explain the x-ray edge "anomalies" observed in these simple metals. This latter subject is treated separately in a following paper, hereafter referred to as II.[1] In the present work we shall restrict ourselves to identifying and interpreting the relevant many-body processes as they apply to XPS line shapes. It will be shown that such analyses provide strong support for an intuitive understanding of many-electron effects in simple metals and, equally important, demonstrate the quantitative success of existing theoretical (and perhaps less intuitive) formalisms which describe their behavior.

Our discussions in this paper center on two distinct types of many-body phenomena in XPS, the creation of electron-hole pairs and the creation of phonons, both upon the sudden removal of a core electron. While phonon generation is well known, it is included here for two reasons. First, in con-

trast to many-*electron* theories, previous models describing this many-*atom* response in simple metals have been much less successful in accounting for observed electron-phonon interactions. Second, determination of accurate empirical magnitudes of electron-phonon effects in XPS will prove to be important in the analyses of the x-ray absorption edges discussed in II. Historically it is the interpretation of the x-ray edge spectra (along with the Kondo problem) which initiated the development of the many-electron theory due to Mahan,[2] and Nozières-DeDominicis[3] (MND). Since we shall be dealing here exclusively with XPS spectra, we will concern ourselves only with those formalisms appropriate for describing XPS line shapes. Their development can be treated without recourse to the MND description.

The theory for describing the many-electron response in XPS has its origin in the work of Anderson,[4] who showed that the ground state of electrons in a metal is orthogonal to the state resulting from the sudden production of a core hole ("the orthogonality catastrophe"). Physically this can be understood as follows. Upon creation of a hole in a free-electron metal, the conduction electrons screen the suddenly created charge and the wave functions of each screening electron become modified to a degree that depends on their proximity to the core hole. The overlap of the new wave-function of each electron with its ground state is very close to but less than unity. Because there are so many of these wave-functions, $\sim 10^{23}$, their product approaches zero. The energy required for the screening process is taken from the kinetic energy of the outgoing photoelectron whose ejection produced the hole. The average kinetic energy of the core photoelectron is somewhat higher than in the absence of the screening because the attractive potential of the hole is itself partially screened, but the spectrum exhibits a "tail" of lower-kinetic-energy photoelectrons because of the energy which goes into the excitation of electron-hole pairs. Hopfield[5] has shown that the strength of the electron-hole excitation processes has the character of an infrared divergence, i.e., the number of e-h pairs created upon the sudden switch-on of a potential becomes infinite as the energy of the e-h pairs becomes infinitesimal. The resulting electron spectrum for an infinitely-long-lived core hole is given by $1/\epsilon^{1-\alpha}$,[4,5] where ϵ is the energy measured from the "no-loss" line position and α is called the Anderson singularity index. This parameter, which describes the nature of the electron-hole interaction, is expressed in terms of scattering phase shifts δ_l by the relation

$$\alpha = 2\sum_l (2l+1)\left(\frac{\delta_l}{\pi}\right)^2 . \qquad (1)$$

According to Eq. (1) α is always positive. The Friedel sum rule limits it to values no greater than 0.5. The $1/\epsilon^{1-\alpha}$ line shape therefore diverges as $\epsilon \to 0$ and has a tail at finite ϵ whose amplitude depends on the magnitude of α.

Since all core holes in metals have finite lifetimes the above description is incomplete. To facilitate comparison with real XPS spectra, Doniach and Šunjić[6] (DS) have obtained an expression for the XPS line shape of the form

$$I(\epsilon) = \frac{\Gamma(1-\alpha)\cos[\frac{1}{2}\pi\alpha + (1-\alpha)\arctan(\epsilon/\gamma)]}{(\epsilon^2+\gamma^2)^{(1-\alpha)/2}} , \qquad (2)$$

which includes the lifetime broadening by convolution. Here Γ is the gamma function, and 2γ the full width at half-maximum (FWHM) of the hole-state Lorentzian line shape. In Sec. III we will discuss some of the general features of the DS line shape and the procedures used to obtain the parameters α and 2γ from experimental data. In Sec. IV we will address the important questions concerning the validity of Eq. (2) at energies well removed from the singularity and the means by which the *intrinsic* character of the XPS tail can be distinguished from *extrinsic* energy losses as the photoelectron travels through the solid. In the initial discussion, the many-electron response in XPS line shapes is assumed to be adequately represented by Eq. (2) over some small range of energy.

The creation of a core hole results in a many-atom response due to the electron-phonon coupling between the initial ground and final ionized states. So long as the electronic transitions are sudden, the Franck-Condon principle applies and the zero-point and thermal fluctuations in the initial state are directly (vertically) projected onto the final state containing the core hole. The resulting Franck-Condon envelope has a Poisson distribution, which in the case of large numbers of phonons is well represented by a Gaussian.[7] At finite T, the total width of the phonon envelope is the product of the zero-point width and a temperature-dependent term that describes the occupation number of higher initial phonon states according to Bose-Einstein statistics. Expressions for the total width vary with the sophistication of the theoretical model, and we shall show that quantitative success in calculating phonon widths has been only very recently achieved in the simple metals. Considerations of the interaction between the finite lifetime of the core hole and the phonon frequency response will be discussed in Sec. IV.

As the above brief discussion shows, both many-electron and many-phonon processes in XPS are not new concepts, and so it might seem surprising that a quantitative discussion would have been so long in coming. At least two factors are responsi-

ble for this. The first is that prior to 1973, experimental limitations on surface preparation and energy resolution in XPS precluded reliable identification of these phenomena. The second reason is that few experimentalists were aware of these phenomena or understood how they would manifest themselves in XPS spectra. Lacking a ready explanation for obvious line asymmetries or broadening, these effects were either explained away as artifacts or as being due solely to extrinsic processes and were simply ignored. The correct identifications of electron-hole pair formation[8,9] and of electron-phonon broadening in XPS spectra of solids[10] have been made only within the last few years. It remains to be demonstrated that the observed effects are truly (solely) intrinsic and that their magnitudes can be determined accurately without interference from the extrinsic processes that were once believed to be wholly responsible for them. The recent improvements in experimental capabilities and data analyses reported in this work now enable these questions to be addressed and subjected to a critical test.

In Sec. II we describe our experimental procedures and in Sec. III present the experimental results and methods for analysing the data. A discussion of the results is given in Sec. IV.

II. EXPERIMENTAL PROCEDURES

X-ray photoemission from Li, Na, Mg, and Al was studied with both HP 5950A ESCA and modified AEI 100 spectrometers. In the former, high-purity (99.99%) samples were repeatedly evaporated onto polished stainless-steel substrates at room temperatures in a sample chamber with base pressure $\sim 10^{-8}$ Torr, then quickly inserted *in vacuo* into the analyzing chamber at a base pressure in the low 10^{-9} Torr region. Because of the concern about surface contamination, spectra were recorded quickly (~5–10 min) at a total energy resolution of 0.63 ± 0.03 eV full width half maximum (FWHM), somewhat lower than the highest resolution of 0.55 eV attainable with that instrument. The source of radiation was monochromatized Al $K\alpha$ x rays. In the AEI instrument, high-purity samples were repeatedly evaporated onto room-temperature stainless-steel substrates in the analyzer region at a base pressure of $\sim 10^{-11}$ Torr. A special Al $K\alpha$ monochromator was developed[11] which allowed a total instrumental resolution of 0.25 ± 0.02 eV, FWHM.[12] The response function of the lower-resolution HP instrument was determined from analysis of Fermi edges from Ag, Au, and Ga, while that of the higher-resolution AEI instrument was determined from detailed analyses of all available core level spectra (see Sec. III for analysis procedures). Both functions were found to be approximately Gaussian.[12,13] While neither procedure for determining the spectrometer functions is by itself rigorous, it will be shown in Sec. III that the limits of uncertainty in the widths and shapes of these functions are negligible compared with other contributions to the observed XPS line shapes.

For the case of Li and Mg, spectra were recorded with the AEI instrument as a function of temperature. High-purity lithium and magnesium were repeatedly evaporated onto smooth room temperature substrates. Mg $2p$ spectra were twice recorded alternately at 90 and 300 °K temperatures. More systematic Li $1s$ measurements at room temperature were made before and after each low- (90 °K) and high- (440 °K) temperature run. Each Li $1s$ data set at low and high temperatures represents the sum of three runs, that at room temperature the summation of all the room-temperature runs. This accounts for the better statistics in the room-temperature spectra.

The Li, Na, and Mg data taken in the AEI instrument typically represent a total of 20 h per spectrum. In spite of these rather long data acquisition times, the very-high-resolution spectra have only ~1% statistics in the best case and ~3% statistics in the worst. While acceptable for most conventional needs, these statistics are well below those required for deconvolution procedures and thus dictate the need for other methods in the analysis of XPS line shapes. These analytical procedures are discussed in Sec. III.

III. EXPERIMENTAL AND ANALYTICAL RESULTS

X-ray photoemission spectroscopy of reactive metals is by now almost routine as a result of advances in ultrahigh vacuum technology. The desire to extract information from the details in the XPS line shape, however, imposes the requirements of extremely high resolution and, at the same time, low statistical uncertainty. This combination is particularly demanding since one is usually achieved at the expense of the other. We shall see that high resolution is the more important of the two, and that analysis of the data requires care over and above conventional standards. In order to appreciate the procedures of the analysis, it is instructive to review briefly the properties of the XPS line shape defined by Eq. (2).

The power-law shape is shown in Fig. 1(a) for the case of $\gamma = 0$ and $\alpha = 0.2$. α is the singularity index defined by Eq. (1) and 2γ is the core-hole lifetime at FWHM. Figure 1(b) shows the DS line shape for different α's but with $2\gamma = 0.5$ eV. Note that, as expected, only the high binding energy (low kinetic energy) side of the peak varies with

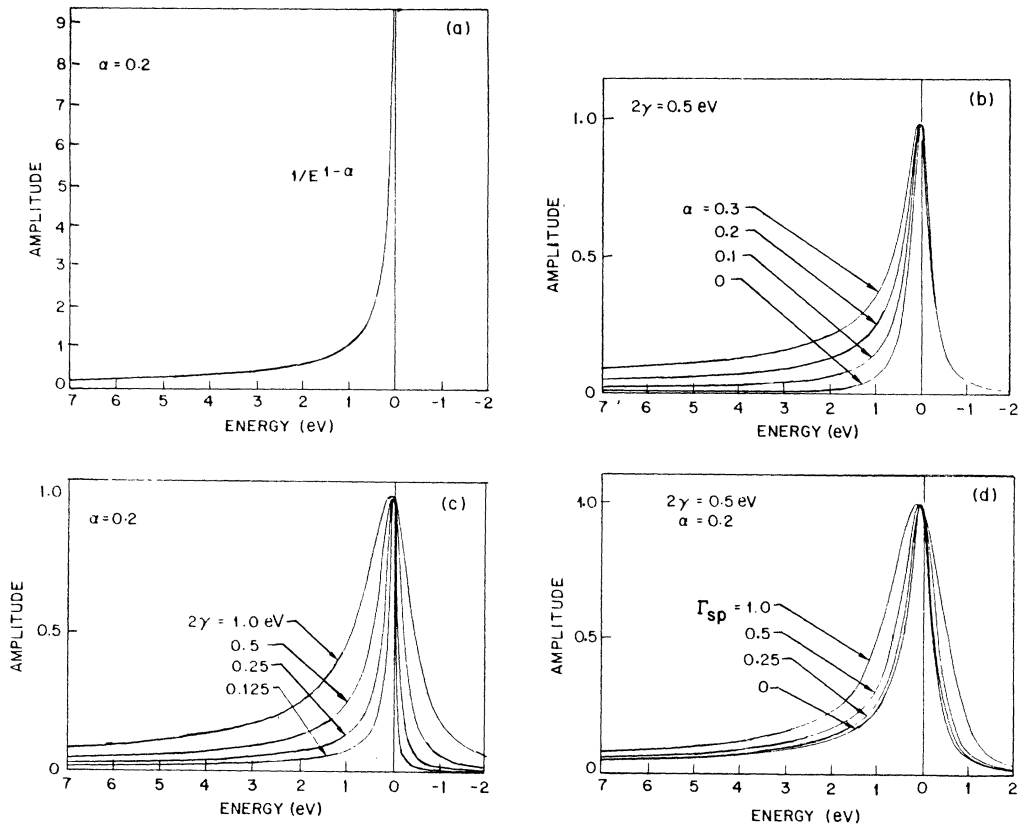

FIG. 1. Theoretical and experimental features of the x-ray photoemission line shape in a free-electron-like metal. (a) Theoretical line shape of infinitely-long-lived core hole showing intrinsic nature of the asymmetric electron-hole-pair tail. (b) Theoretical Doniach-Šunjić (DS) line shape of core hole with FWHM lifetime width of 0.5 eV and various values of singularity index α. Note small binding energy shift from (a) and insensitivity of right side of peak to different values of α. (c) Theoretical DS line shape with constant α and varying core hole lifetimes. Note both right and left sides of peak are affected by changing lifetime. (d) Typical *experimentally* observed DS line shape of constant singularity index and core-hole lifetime, but with varying spectrometer response function FWHM widths, Γ_{sp} shown here to be Gaussian. Note strong dependence of line shape to changing values Γ_{sp}, illustrating importance of including Γ_{sp} in data analysis.

changing α. Figure 1(c) contains a series of line shapes for $\alpha = 0.2$ and different γ's, showing how both high- and low-energy sides of the peak vary. This too is expected because the Lorentzian contribution of the hole lifetime is symmetric about $\epsilon = 0$.

The asymmetric tail in Figs. 1(a)–1(c) extends a good deal beyond $\epsilon = 2\gamma$ and increases noticeably with increasing α. Much of the area associated with this line shape is contained in the tail, so that for accurate quantitative analyses this total intensity must be taken into account.[14] The tail is seen to be an intrinsic property of the XPS line shape and should therefore not be confused with extrinsic energy losses. This point is clearly very important in the analysis of the XPS data because if a "background" is subtracted before fitting theory to experiment, the resulting singularity index will be in error—if the line can be fitted at all. It is therefore crucial to determine to what extent extrinsic losses, which are *always* present in an XPS spectrum, contribute to the observed line shape. To allow a logical development of our analytical procedures we will defer this question to Sec. IV. For the present we state without proof that the tail is indeed predominantly intrinsic up to $\epsilon \sim \frac{1}{2}E_F$ and that "background subtraction" in metals is an inherently incorrect procedure in this energy regime.

The line shapes of Eq. (2), shown in Figs. 1(b) and 1(c), are functions of ϵ/γ with the single parameter α. It is therefore possible to characterize them by other individual properties, such as the ratio x of the half-width-at-half-maximum (HWHM) values of the higher- and lower-binding-energy sides of the peak. This was originally suggested by Doniach and Šunjić and a table relating x and α is given in their work. Unfortunately, the

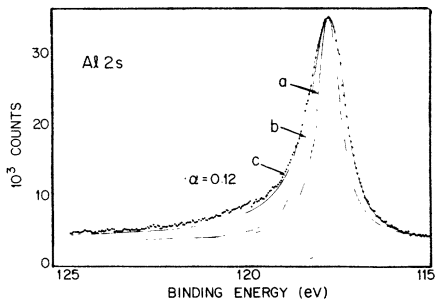

FIG. 2. Al 2*s* x-ray photoemission spectrum illustrating stepwise procedures in visual data analysis. Curve *a* is pure lifetime Lorentzian with FWHM of 0.78 eV, $\alpha = 0$. Curve *b* is curve *a* convoluted with skewed-Gaussian instrumental response function (see Ref. 13) with FWHM of 0.63 eV. Curve *c* is curve *b* but with $\alpha = 0.12$. Note presence of surface oxide ~2.7 eV from main peak which limits analysis from these data (measured at 10^{-9} Torr).

ideal line shapes in Figs. 1(b) and 1(c) are not experimentally observable because there is always some broadening due to the response function of the spectrometer. Assuming a Gaussian spectrometer function and denoting the FWHM by Γ_{sp}, we show in Fig. 1(d) the curves in Fig. 1(b) broadened by $\Gamma_{sp} = 0.5$ eV. It is clear by inspection that in going from Fig. 1(b) to 1(c) or 1(d), the parameter x does not retain its functional relationship with α because the broadening of an asymmetric function by even a symmetric one results in a change in asymmetry.

In order to obtain the intrinsic parameters α and γ it is thus imperative to take into account *all* additional broadening. One way to do this is by deconvolution. Early attempts with this method were only moderately successful[15] because removal of the majority of the broadening requires data with better statistics and a better knowledge of the resolution function. A more practical approach is to include all of the broadening in the function that is to be fitted to the data, i.e., to convolute the DS function with the resolution function (and the phonon broadening). This leads to considerable complications, however, because the fitting function is then no longer available in closed form, making numerical evaluation tedious.

Two methods for analyzing the data were therefore developed. The first involves a visual comparison of the raw experimental data with the result of a computer-generated DS line shape that has been convoluted with the instrumental response function.[16,17] If the latter function is known, the only significant parameters in the analysis are α and γ (the position and height of the peak do not influence the shape). This procedure has the particular advantage of readily identifying any possible traces of surface oxide which appear on the high-binding-energy side of the peak. It has also been most useful for obtaining initial parameters for the second method of analysis described below using a least-squares fitting routine.

As an illustrative example of the visual procedure we consider the XPS spectrum of Al 2*s* electrons, shown in Fig. 2. The data were obtained with the lower-resolution HP spectrometer. As we have seen from Fig. 1(b), the right-hand side of the peak is sensitive only to γ whereas the left-hand side of the peak is sensitive to both γ and α. The method of attack is thus to first determine γ. In practice this is done by choosing arbitrary values of γ and α in Eq. (2), convoluting the resulting function with the spectrometer response, and comparing the final result with the right-hand side of the peak; γ is then varied until agreement is obtained. α is determined the same way but now with fixed γ. To show what the various steps in the procedure look like by themselves we exhibit them in Fig. 2: curve *a* is a Lorentzian of $2\gamma_{2s} \equiv \Gamma_{2s} = 0.78$ eV, $\alpha = 0$; curve *b* is curve *a* broadened by the spectrometer function, $\Gamma_{sp} = 0.63$ eV; curve *c* is curve *b* but with $\alpha = 0.12$. Comparison of the data with curve *c* shows excellent agreement on the low-binding-energy side, but on the high-binding-energy side the presence of a small amount (<0.3 monolayer) of surface impurity centered at ~2.7-eV higher binding energy is apparent. The impurity was determined to be Al_2O_3 from the observed O 1*s* spectra and its steady growth with time which matched the growth of the Al impurity signal. The presence of this impurity, however small, clearly introduces some uncertainty and is the limiting factor in determining α from these data.

In Fig. 3 we show an Al 2*p* spectrum taken with the higher-resolution instrument. The improved vacuum conditions provide data without observable indication of surface impurity. The Al $2p_{3/2}$ and Al $2p_{1/2}$ components are clearly resolved and allow the data to be analyzed following our previous prescriptions. If we constrain the spin-orbit component intensities to 2:1 and allow their splitting to vary, a visual best fit is obtained with a splitting of 0.40 ± 0.01 eV, a 2*p* lifetime $\Gamma_{2p} = 0.04 \pm 0.02$ eV, and a singularity index $\alpha = 0.115 \pm 0.015$. The uncertainty in determining α is illustrated in Fig. 3 by the expanded region, where the limits in α of ± 0.02 are clearly seen to be too large.

The second, more direct, and less subjective procedure for analyzing the data is to perform a nonlinear least-squares adjustment to the parameters in this function for optimum fit to the raw experimental data. We have used a program due to Marquardt[18] for this purpose, and found that it

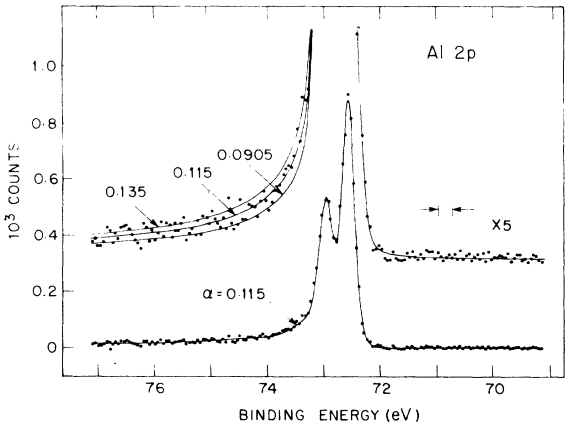

FIG. 3. Al $2p_{3/2}$ and Al $2p_{1/2}$ x-ray photoemission spectrum, illustrating limits of less than ± 0.02 uncertainty in α from analysis of this data using procedures outlined in text and Fig. 2. Data measured in 10^{-11} Torr vacuum with high-resolution spectrometer (FWHM width shown in upper right). Note absence of observable surface oxide (contrast with Fig. 2).

converges rapidly provided good starting parameters are used. It is, of course, also essential to include such features as the bulk and surface plasmons (and surface oxide, if any) in the theoretical function if a meaningful fit is to be obtained. Furthermore, the ability to constrain, say, the widths, asymmetries, and peak-height ratio of closely spaced spin-orbit components is also of great value. In some respects the resolution function presents the most troublesome aspect in this procedure. While there can be little question, in view of the central-limit theorem, that a Gaussian should provide the most reasonable one-parameter closed-form representation, there is also no reason to expect the resolution function to be strictly symmetrical.[12,19] Careful analysis of line shapes during the course of this work has shown that a Gaussian one-parameter representation is generally a good one for much of the data analyzed here. Any deviations from this functional form will be explicitly pointed out when appropriate.

It is important to demonstrate explicitly that our least-squares fitting procedure is capable of readily distinguishing between Gaussian and Lorentzian widths. To this end we have analyzed the Al $2p$ spectrum of Fig. 3 over a 6-eV interval, extending from 1.5-eV ($\sim\frac{1}{8}E_F$) higher binding energy from the $2p_{3/2}$ line to 4.5-eV lower binding energy, using a flat background and two lines with identical shape and 2:1 intensity ratio to represent the spin-orbit doublet. A series of fits were made in which the Gaussian component, representing the instrumental and phonon contributions (to be discussed), was constrained to fixed values. The result, Fig. 4, shows a clear minimum in χ^2 for a Gaussian width of 0.234 ± 0.006 eV, and indicates that the lifetime width of the $2p$ hole state is $0.045^{+0.006}_{-0.010}$ eV. Two different error bars are shown in this figure. The inner ones represent a "one-parameter" standard deviation, calculated with all other parameters held fixed at their best-fit values. The outer error bars are "support plane" limits obtained from the tangent planes to the N-dimensional error surface and contains the effects of parameter correlations.[18] The singularity index α is a weak function of the Gaussian width in this case because the total width is dominated by the Gaussian contribution.

This method of analysis, in which one displays a

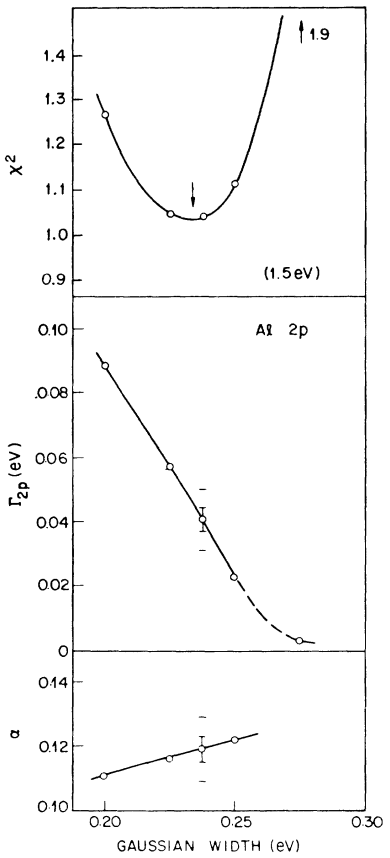

FIG. 4. Results of nonlinear least-squares analysis of Al $2p$ data in Fig. 3, showing χ^2 (upper), Al $2p$ hole lifetime at FWHM (middle), and α (lower), all as a function of FWHM Gaussian width. Gaussian function represents instrumental response and effects of phonon broadening. Data were fit over range of 1.5-eV binding energies from Al $2p$ peaks. Minimum in χ^2 is indicated by arrow, and limits of uncertainty in α, Γ_{2p}, and Gaussian width are thus small. Standard deviations and support plane limits of values are indicated by inner and outer horizontal bars, respectively. Note agreement between α determined here and that in Figs. 2 and 3.

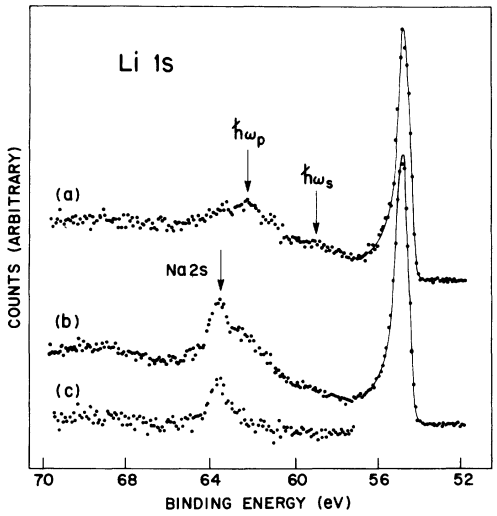

FIG. 5. Li 1s x-ray photoemission spectra from high-purity Li evaporated onto substrates at (a) 90 °K and (b) 300 °K. Surface segregation of Na at 300 °K is seen in Na 2s spectrum shown in (c), obtained by subtracting (a) from (b). Bulk and surface plasmons at 7.20 and 4.15 eV, respectively, are also indicated. Note that in (a) $\hbar\omega_s$ is significantly (and unexplicably) smaller than $\hbar\omega_p/\sqrt{2}$, even though surface Li is atomically clean.

cut through the n-dimensional χ^2 surface, is particularly helpful in gaining a physical feeling for the quantitative interrelationship of the parameters that are adjusted in the least-squares procedure. It is, of course, not necessary to carry this out in detail since the Gaussian-width parameter can also be directly adjusted by the least-squares procedure, and comparable information is available in the parameter correlation coefficients. Nevertheless, this method is particularly useful in the case of Li for demonstrating the temperature dependence of the Gaussian component (see below).

The most significant aspect of the above analyses of the Al 2p and Al 2s results is that from spectra of core levels whose hole lifetimes differ by more than an order of magnitude taken with spectrometers whose resolution differ by a factor of 2.5 and which have been analyzed by two different techniques, we have determined a value for α that is consistent within a conservative experimental uncertainty of ± 0.015. This clearly demonstrates that our analysis procedures are generally valid. We note also that our result is inconsistent with the value of $\alpha = 0.161 \pm 0.008$ quoted by Ley *et al.*,[20] who determined α by measuring the parameter x after subtracting a background from the raw data in which the spectrometer broadening was not taken into account.

There is an additional phenomenon which may affect the XPS line shape, namely phonon broadening. It's FWHM value is denoted by Γ_{ph}^{XPS}. The coupling constant is usually sufficiently large to assume a Gaussian rather than a Poisson phonon distribution function (this point will be discussed in Sec. IV B). Thus it should be possible to observe an additional Gaussian broadening in the data, provided it is not completely dominated by the broadening from the spectrometer.

To illustrate the most dramatic effects of phonon broadening, we consider the case of lithium. In Fig. 5(a) we show a 15-eV sweep of Li evaporated and measured on a substrate at $T = 90$ °K. The bulk and surface plasmons are indicated at 7.20 ± 0.1 eV and 4.15 ± 0.1 eV, respectively. The surface purity of the samples measured in these experiments is extremely high as determined from the virtually complete absence of XPS core level signals from impurity elements. It comes as a surprise, therefore, that the surface plasmon energy, which agrees well with other literature values,[21-23] is so different from the value of 5.1 eV ($=\hbar\omega_p/\sqrt{2}$) predicted from a free-electron model. This discrepancy has already been noted by Kloos[21] in his measurements made under somewhat poorer vacuum conditions, and still remains to be explained. Our value of the bulk plasmon energy is in fair agreement with that of Kloos,[21] 7.08 eV, but the literature values range from 6.94 to 9.5 eV.[24] If the sample at 90 °K shown in Fig. 5(a) is allowed to warm up to room temperature and is then remeasured, the spectrum shown in Fig. 5(b) is obtained. The difference spectrum between Figs. 5(a) and 5(b) is shown in Fig. 5(c), indicating the presence of Na 2s photoelectrons. The Li samples used are quoted as containing less than 60-ppm Na, but in addition to the Na 2s spectrum in Fig. 5(c) the other core and Auger lines of Na, not shown, were also observed. Fortunately, the presence of Na surface segregation is not a problem in our analysis of the Li 1s line shape since its effects, which occur more than 7 eV from the main line, are well removed from the region of interest covering ~1.5 eV.

In Fig. 6 we show a 10-eV scan of the Li 1s region taken at 300 °K with the high-resolution instrument. If we apply to Li the analysis procedures outlined above for the Al 2p and Al 2s spectra (in which the effects of phonon broadening were ignored), we obtain the result shown in Fig. 6(a). Bulk and surface plasmons approximated by Lorentzians of variable height and width have also been included. Although the fit is quite good on the high-binding-energy side of the peak, it is clearly unsatisfactory on the low-energy side and thus shows the need for another approach. If, instead, we follow our original procedures but now include

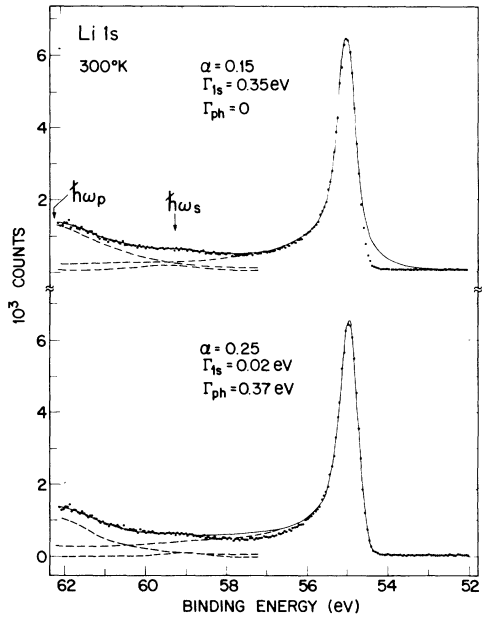

FIG. 6. Li 1s x-ray photoemission at 300 °K. In upper spectrum, data is fit with DS line shape plus two Lorentzians for plasmons. Note Lorentzian lifetime width of the Li 1s hole-state is too large, giving poor fit. In lower spectrum, additional Gaussian is convoluted with DS line shape containing smaller Lorentzian lifetime width. Note improvement in fit on *both* sides of peak. Deviation in fit above ~1.5 eV from peak is due to inapplicability of DS line shape in Li (see Sec. IV C).

an additional Gaussian broadening, we obtain the result shown in Fig. 6(b). The deviation of the fit to the data above ~1.5 eV from the main peak is due to the limited region of applicability of the DS function and is discussed in more detail in Sec. IV C. Within the ±1.5 eV range on both sides of the peak, however, the result is clearly improved.

We consider the need for the additional broadening in Fig. 6(b) to be evidence for the effects of phonons.[17] That phonons are indeed responsible is demonstrated by the temperature dependence shown in Fig. 7. As the temperature is increased from just above liquid nitrogen, to ambient, to just below the Li melting point a sizable increase in the measured widths of the Li 1s peaks is observed. Since the spectrometer function is not strongly temperature dependent and the Li 1s lifetime is at most only very weakly sensitive to temperature changes, the width of the additional broadening can be determined by treating the lifetime and spectrometer widths, Γ_{1s} and Γ_{sp}, as constants and varying the phonon width Γ_{ph}^{XPS}. Setting $\Gamma_{1s} = 0.04$ eV (see below) and assuming that the phonon broadening is Gaussian, the resulting fitted line shapes (shown as solid lines) and the corresponding values of Γ_{ph}^{XPS} and α at different temperatures are indicated in Fig. 7. The data are fit extremely well by these line shapes, supporting our assumption of a Gaussian function for the phonon broadening. (The assertion that this temperature dependent broadening is, in fact, due to phonons and should be Gaussian will be defended more rigorously in Sec. IV B.)

The reason for our choice of $\Gamma_{1s} = 0.04$ eV from

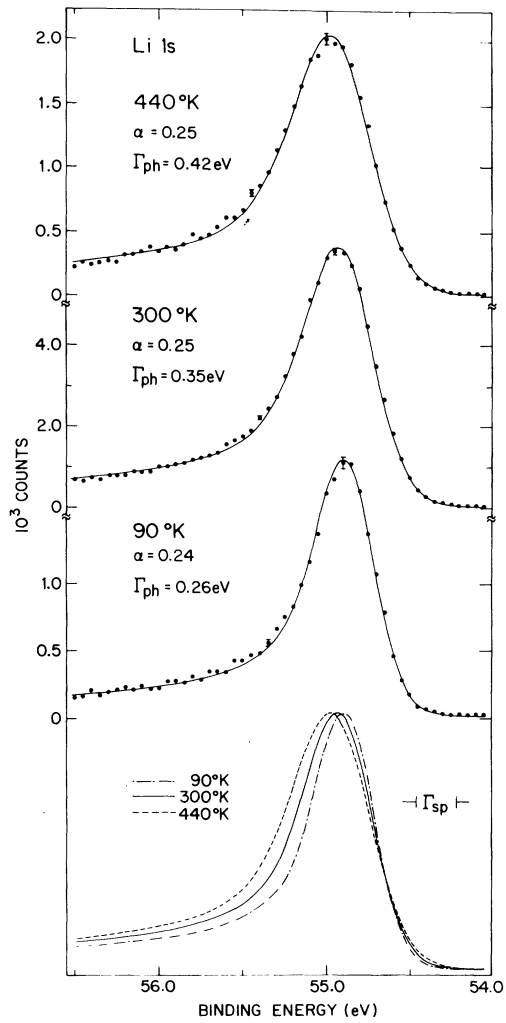

FIG. 7. Li 1s x-ray photoemission as a function of temperature. Data (points) are fit (solid lines) using procedures described in lower spectrum of Fig. 6 and in text assuming constant Li 1s lifetime width $\Gamma_{1s} = 0.04$ eV (see Fig. 8) but variable α. Gaussian phonon widths at FWHM were determined assuming Gaussian spectrometer function with $\Gamma_{sp} = 0.25$ eV. Note essential constancy of α but large increase in Γ_{ph} with increasing temperature, illustrating importance of phonon broadening. At bottom, fits at different temperatures are overlaid to emphasize increased broadening and increased Li 1s binding energy at elevated temperatures.

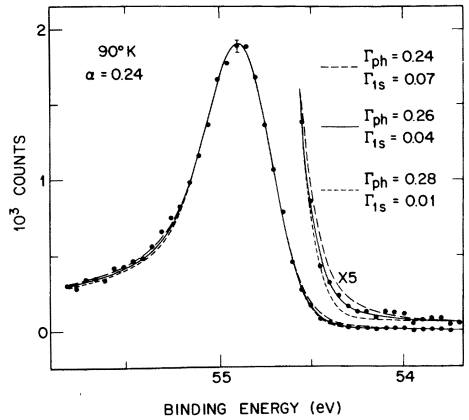

FIG. 8. Li 1s x-ray photoemission spectrum at 90 °K showing limits of uncertainty in determining lifetime width, Γ_{1s}, and phonon width, Γ_{ph}, in eV at FWHM for given singularity index $\alpha = 0.24$ and Gaussian spectrometer width $\Gamma_{sp} = 0.25$ eV. From this method of analysis (see bottom Fig. 6 and text) best values are $\Gamma_{ph} = 0.26 \pm 0.02$ eV and $\Gamma_{1s} = 0.04 \pm 0.03$ eV.

the visual analysis procedure of the data is illustrated in Fig. 8, where we show the Li-1s data at 90 °K fitted with line shapes of variable values of Γ_{1s} and Γ_{ph}^{XPS}. The tail region on the low-binding-energy side of the data should be most important in distinguishing the relative contributions of the long-tailed Lorentzian lifetime function and the short-tailed Gaussian phonon function. Limits of uncertainty can be determined for the two components by requiring that the resulting line shape above the FWHM points fit the data uniformly well for any combination of Γ_{1s} and Γ_{ph}^{XPS}. This requirement therefore allows one component to be adjusted at the expense of the other and serves to constrain the limits of each. From the expanded tail region shown in Fig. 8 it is clear that the values $\Gamma_{1s} = 0.04$ eV and $\Gamma_{ph}^{XPS} = 0.26$ eV comprise the most acceptable combination and that the uncertainties of ±0.02 eV for each value appear to be reasonable limits. The above analysis was performed assuming a constant Gaussian spectrometer width of $\Gamma_{sp} = 0.25$ eV.

The presence of large Gaussian broadening well above the instrumental resolution function has also been readily demonstrated by least-squares analysis. The data were fitted over a 4-eV interval, starting 3 eV below the binding energy of the 1s peak and using a single DS line convoluted with a Gaussian to represent the combination of the instrumental and phonon broadening. Least-squares adjustments were made with the Gaussian width held fixed to a series of values ranging from the instrumental resolution function to the width of the line in the data. A minimum in χ^2 for each spectrum at the three different temperatures was obtained, which defines the phonon broadening, the lifetime width, and the singularity index. The minima correspond to consistent values of α near 0.25 and give phonon widths in excellent agreement with our earlier results obtained from the visual analysis procedure.[17] Because of the shallower minimum in χ^2 compared with that for Al 2p, see Fig. 4, the Li 1s lifetime width is less well determined. Inspection of the error bars from the fits, however, places a clear upper limit on Γ_{1s} of 0.06 eV.

The singularity index α for Li obtained from the analysis in Figs. 7 and 8 is found to be essentially invariant with temperature, as theory requires. Taking into account all three temperature measurements and the uncertainties in Γ_{1s} and Γ_{ph}^{XPS}, we obtain a mean value of the Li singularity index $\alpha = 0.250 \pm 0.010$. We should mention at this point that in both the visual and least-squares analysis of the Li 1s data described above we have assumed a symmetrical Gaussian spectrometer function with FWHM of $\Gamma_{sp} = 0.25 \pm 0.02$ eV. Detailed inspection of Au and Ag core-level line shapes taken near the time of the measurements of the Li 1s spectra showed a slight skewing in the Gaussian instrumental response function. We have investigated the effects of this by a least-squares refitting of all the Li 1s data using a two-parameter skewed Gaussian representation.[13] The phonon and lifetime widths were found to decrease and increase with respect to the results obtained in the aforementioned analysis by no more than about 0.02 eV, i.e., within the uncertainty limits of the assumed Gaussian function. The singularity indices, however, were uniformly lower than the value of 0.25 by about 0.03. Since the skewed Gaussian spectrometer function used represents a somewhat extreme case, we feel confident in quoting the lifetime and phonon values determined with a Gaussian response to have uncertainty limits of no more than ±0.03 eV and the singularity index to have a mean value of $\alpha = 0.23 \pm 0.02$.

A final feature in the temperature-dependent Li-1s measurements is a small but reproducible increase in binding energy with increasing temperature. The energy displacements in going from 90 to 300 °K and from 300 to 440 °K are 0.025 ± 0.005 and 0.040 ± 0.005 eV, respectively. The origin of the shifts lies in a combination of anharmonic nuclear motions and a temperature dependent electronic relaxation, and will be discussed in more detail in Sec. IV B.

Thus far we have analyzed the Al 2p and 2s spectra to illustrate the essential procedures for extracting the singularity index and the lifetime values, and have analyzed the Li 1s spectra to illus-

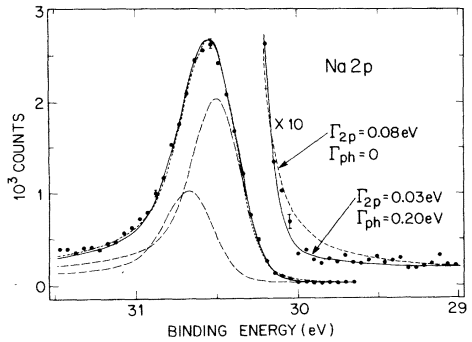

FIG. 9. Na $2p$ x-ray photoemission spectrum at 300 °K showing existence of photon broadening in Na. Dashed line is DS function without phonon broadening and $\alpha = 0.20$, solid line is same curve but with smaller lifetime width convoluted with Gaussian of FWHM $\Gamma_{ph} = 0.20$ eV. Spin-orbit $2p_{3/2}$ and $2p_{1/2}$ components (unresolved) are also shown.

trate the need for also including phonon broadening. It is therefore appropriate to reconsider the Al $2p$ spectrum at 300 °K in Fig. 3 to see how important phonon broadening is in that metal as well. From Fig. 4 we saw that a total Gaussian component with FWHM of $\Gamma_{tot} = 0.234 \pm 0.006$ eV best fit the data. Since this total Gaussian includes the effects of phonon broadening, to determine its magnitude we must first know the smallest possible spectrometer broadening of the modified instrument. The theoretical lower limit of Γ_{sp}(min) is 0.20 eV,[11] so the maximum phonon component Γ_{ph}^{XPS}(max) = $[\Gamma_{tot}^2 - \Gamma_{sp}^2\ (\text{min})]^{1/2} = 0.12 \pm 0.01$ eV. As will be discussed in Sec. IV B, the minimum phonon broadening in Al for photoemission of Al $2p$ electrons arises from the recoil broadening of the ion in the lattice[25] and is calculated to be Γ_{ph}^{XPS}(min) = 0.09 eV. We therefore determine $\Gamma_{ph}^{XPS} = 0.11 \pm 0.02$ eV for Al. This value is considerably smaller than that for Li at 300 °K, 0.37 ± 0.03 eV, but is still not negligible compared to kT and therefore should not be ignored in cases where the instrumental resolution is comparable to kT. In these XPS experiments, the FWHM of even the high-resolution spectrometer function is approximately $10kT$ at $T = 300$ °K and cannot be expected to remain constant throughout all the measurements.[12] Therefore, in determining the Gaussian phonon contribution to the core-level line shapes, it is necessary to evaluate Γ_{sp} for each series of measurements.

The phonon broadening in Na is qualitatively determined using the above visual procedures applied to the expanded Na $2p$ spectrum shown in Fig. 9. [In an earlier analysis,[16] the lower-binding-energy side of the expanded Na $2s$ spectrum was fit well by lifetime and spectrometer broadening alone, but the short Na $2s$ lifetime effectively obscured the phonon broadening contribution. This led to a somewhat smaller value of α than that reported here (see below).] The importance of phonon broadening can be seen in Fig. 9 by first ignoring its contribution and attempting to fit the lower-binding-energy tail of the expanded Na $2p$ peak while constraining the fit at and above FWHM; an obviously unsatisfactory result is obtained, see dashed curve. Including phonon broadening by convolution of a DS function with an additional Gaussian phonon width $\Gamma_{ph}^{XPS} = 0.20$ eV and a longer Na $2p$ lifetime results in a distinct improvement.

Least-squares analysis allows for a more quantitative determination of the phonon broadening in both the Na $2s$ and $2p$ spectra. Using the procedure described above, we obtained minima in χ^2 shifted well away from the 0.25-eV instrumental Gaussian[12] in both cases. This is a particularly instructive result because, in spite of the order-of-magnitude difference in lifetime widths between the Na $2p$ and Na $2s$ holes, consistent values for the Gaussian width and the singularity index were obtained. Using the value of $\Gamma_{sp} = 0.25$ eV, we find Γ_{ph}^{XPS} equal to 0.18 ± 0.01 and 0.20 ± 0.01 eV for Na $2p$ and Na $2s$, respectively. Including the uncertainty of ± 0.02 eV in Γ_{sp} increases the error limits to ± 0.03 eV. Note that as for Al, Γ_{ph}^{XPS} is appreciably smaller than that for Li but is nonetheless significantly larger than kT and should not be ignored.

To determine α for Na it is necessary to analyze both the $2p$ and $2s$ spectra shown in Figs. 9 and 10, respectively. The presence of a trace amount (~0.1 monolayer) of oxidized Na (due to oxide-leaching of the vacuum-sealed glass vial containing the Na) is seen at ~1 eV higher binding energy above the Na $1s$ peak in Fig. 10. This information is used to extract α from no more than ~1 eV ($0.3E_F$) above the binding energy in the Na $2s$ spectrum. The influence of the surface plasmon, also shown in Fig. 10, is seen to be negligible within 1 eV from the peaks. After convolution of the phonon broadening term (see Fig. 9), a best value of $\alpha = 0.20 \pm 0.015$ for both $2p$ and $2s$ levels is obtained. (In Sec. IV C we will also show that the essential equivalence of α values for the Na $1s$ and $2s$ spectra in Fig. 10 is direct evidence for the intrinsic nature of the asymmetric e-h pair tail.)

As a final check on the values of α we have carried out a least-squares analysis of all three sets of Na data and the results are shown in Fig. 11. In each case the phonon width was treated as a free parameter. The Na $2p$ data were fitted over a range of 2.5 eV from the peak with the spin-orbit splitting held at the free-ion value of 0.169 eV and the intensity ratio of the components held at 2:1. The oxide surface contamination had to be explicitly

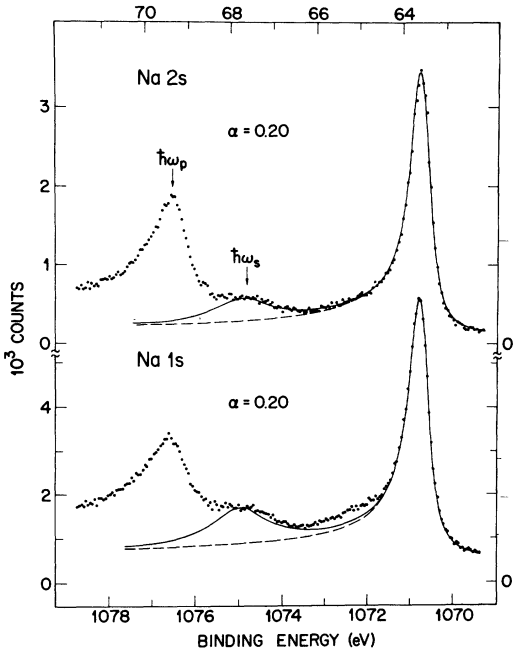

FIG. 10. Na 2*s* and Na 1*s* x-ray photoemission spectra, at 300 °K showing direct evidence for intrinsic nature of asymmetric electron-hole-pair tail near peak. DS function (solid line) was fit to the data up to ~1 eV from peak and was then extended beyond (dashed line). To it was added a Lorentzian at surface plasmon energy $\hbar\omega_s$. In spite of plasmon and trace surface oxide at ~1 eV from main peak (more visible in 1*s* spectrum due to smaller photoelectron escape depth; also note larger surface plasmon intensity), α values are identical for different core levels.

included in the model. The relatively broader Na 2*s* data were insensitive to the trace surface oxide and were readily fitted over the entire range of 7.0 eV by simply including the bulk and surface plasmon in the model equation. The Na 1*s* data, on the other hand, required explicit consideration of the surface oxide (due to the smaller Na 1*s* electron escape depth), but gave a good fit and consistent numerical results when that was done.

Similar least-squares analysis of the Mg 2*s* and 2*p* data are shown in Fig. 12. The instrumental response function during the course of the Mg measurements was found to be best approximated by a skewed Gaussian.[12,13] The Mg 2*p* and 2*s* data showed no evidence of surface contamination, and the data were analyzed over a range extending 3 eV ($0.4E_F$) above the binding energy of the respective peaks. The analysis of Mg 1*s* data, for which the electron escape depth is comparitively small, did lead to anomalously large values of α. However, analysis of several Mg spectra recorded at various times suggested that this result was un-

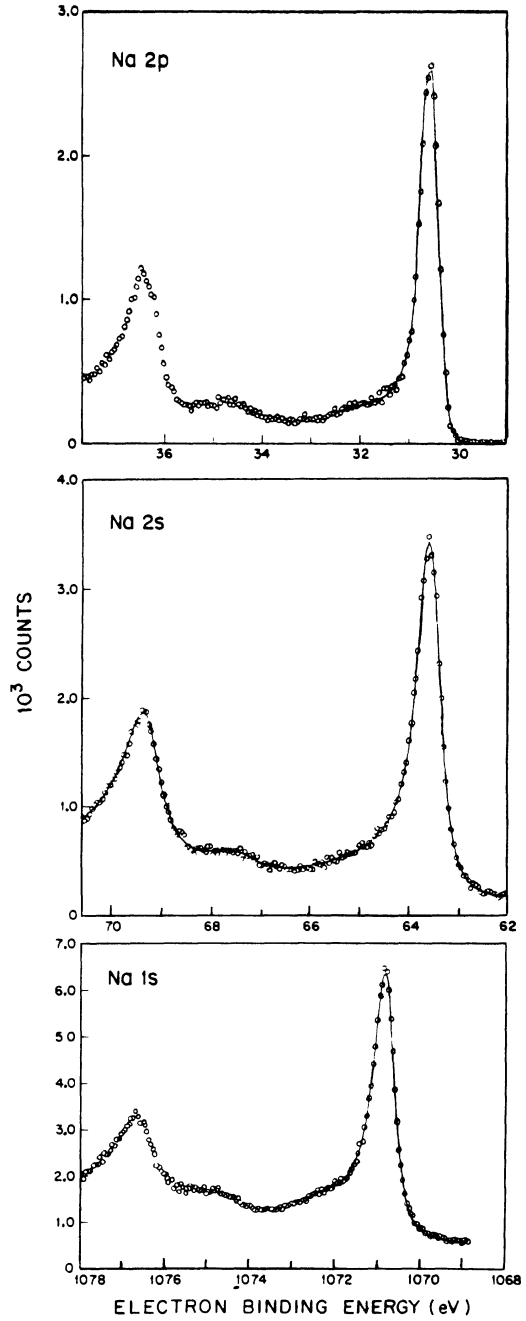

FIG. 11. Nonlinear least-squares fits to Na 2*p*, 2*s*, and 1*s* x-ray photoemission spectra at 300 °K. In Na 2*p* and 1*s* fits, shown as solid lines, additional surface oxide component was explicitly included whose integrated intensities relative to main peaks were found to be 2.4% and 7.2% at 1.1 and 1.3 eV higher binding energies, respectively. Na 2*s* spectrum was fit over the entire energy range shown including both bulk and surface plasmons (trace surface impurity is unobservable). In all three spectra values of phonon broadening and α consistent with each other and with other analyses (see Figs. 9 and 10) were obtained.

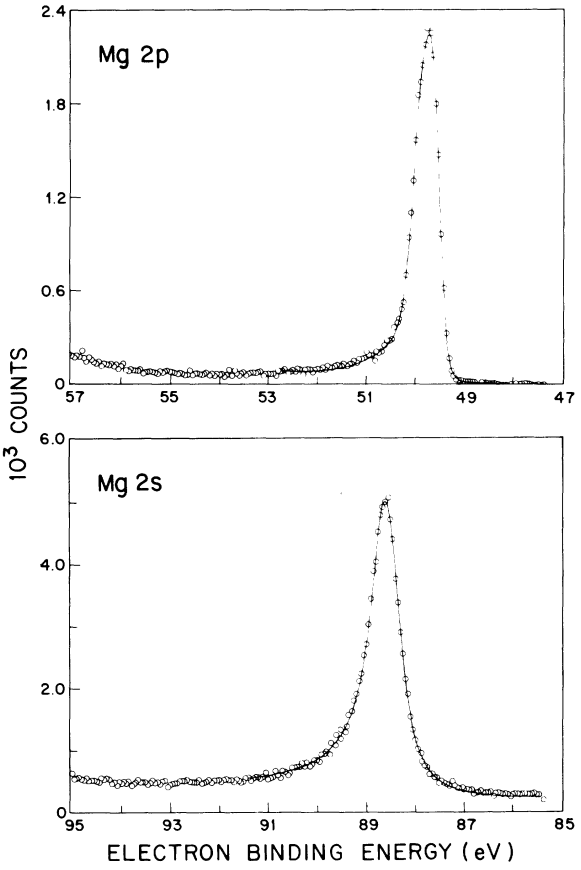

FIG. 12. Nonlinear least-squares fit to Mg $2p$ and $2s$ x-ray photoemission spectra at 300 °K. Data were fit over region indicated by solid lines. Both spectra gave α and Γ_{ph} values consistent with each other and with previous analyses (Ref. 16). Analysis of Mg $1s$ data (not shown) gave anomalously large α value because of small but unresolvable contribution of surface oxide.

doubtedly due to a small but unresolved contribution of surface contamination.

The effects of phonon broadening in magnesium are illustrated in the Mg $2p$ spectra recorded at 90 and 300 °K, see Fig. 13. The data were analyzed by our least-squares fitting routine with variable spin-orbit splitting but fixed 2:1 intensity ratios of the $\frac{3}{2}$ and $\frac{1}{2}$ components. The resulting parameters were used to generate the solid curves. Although the values α, Γ_{2p}, and spin-orbit splittings were virtually identical at the two temperatures, 0.13, 0.03, and 0.28 eV, respectively, the phonon widths are similar but distinctly different. (Gratifyingly the spin-orbit splittings at the two temperatures are found to be equal to each other and to that in the free ion.) Inspection of the 90 °K data reveals a slight improvement of the resolution of the spin-orbit components, and superposition of the fitted curves at the bottom of Fig. 13 indicates a slightly narrower line shape at the lower temperature. These results, while probably pushing the demonstration of the temperature dependence of phonon broadening as far as possible with the present instrumental resolution, confirm the general nature of the more gross phonon effects observed in Li.

Table I summarizes the lifetime, phonon, and singularity values for the simple metals obtained from our analyses of XPS line shapes. Whenever possible, the mean values from the least squares procedures are quoted. Error limits are conservatively rounded off and include all the known *cumulative* uncertainties in the data analyses. The implications of their magnitudes are discussed in Sec. IV.

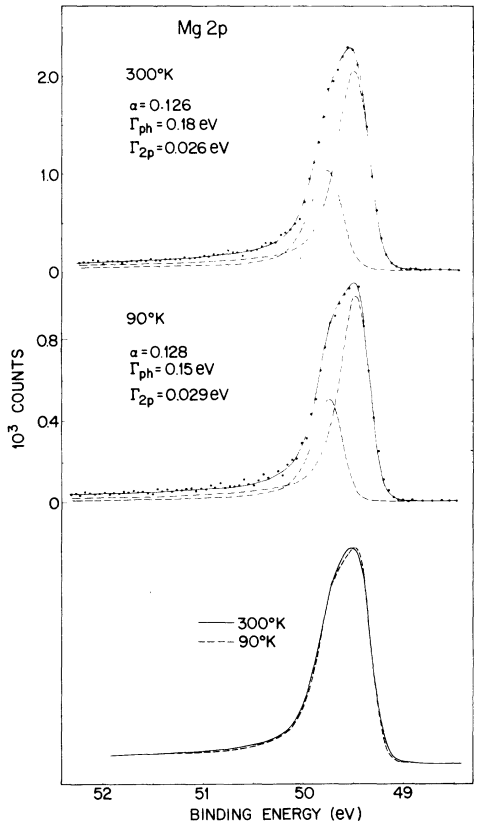

FIG. 13. Mg $2p$ x-ray photoemission spectra 90 and 300 °K showing phonon broadening in Mg. Values of α, Γ_{2p}, and Γ_{ph} determined by nonlinear least-squares fit to both Mg $2p$ data sets were used in generating the expanded and normalized spectra shown here. Note decrease of Γ_{ph} and improved resolution of spin-orbit components (split by 0.28 eV) with decreasing temperature.

TABLE I. Summary of x-ray photoemission results. [a]

Metal		Temp. (° K)	$\Gamma_{n\ell}$ [b] (eV)	Γ_{ph}^{XPS} [c] (eV)	α [d]
Lithium	1s	90	0.04 ± 0.02	0.26 ± 0.03	0.23 ± 0.02
		300	0.03 ± 0.03	0.37 ± 0.03	0.23 ± 0.02
		440	0.03 ± 0.03	0.42 ± 0.03	0.23 ± 0.02
Sodium	2p	300	0.02 ± 0.02	0.18 ± 0.03	0.198 ± 0.015
	2s	300	0.28 ± 0.03	0.20 ± 0.03	0.205 ± 0.015
	1s	300	0.28 ± 0.03	0.18 ± 0.04	0.21 ± 0.015
Magnesium	2p	90	0.03 ± 0.02	0.15 ± 0.04	0.128 ± 0.015
		300	0.03 ± 0.02	0.18 ± 0.04	0.126 ± 0.015
	2s	300	0.46 ± 0.03	0.19 ± 0.04	0.130 ± 0.015
	1s	300	0.35 ± 0.03	0.20 ± 0.05	0.15 ± 0.02
Aluminum	2p	300	0.04 ± 0.02	0.11 ± 0.02	0.118 ± 0.015
	2s	300	0.78 ± 0.05	•••	0.12 ± 0.015

[a] Mean values are quoted and are based on both least-squares analysis and computer-generated comparisons as described in text. Uncertainties include all known cumulative errors of precision from data and from analysis procedures.

[b] Lifetime of n_l hole state, FWHM value.

[c] Phonon broadening measured in XPS, FWHM value. Includes both electronic and recoil phonon broadening, see Eq. (5).

[d] Singularity index.

IV. DISCUSSION

This section is divided into four subsections which deal, respectively, with (A) core hole lifetimes, (B) phonons and other temperature-dependent phenomena, (C) applicability of the DS function to XPS spectra, and (D) singularity indices—all as they pertain to the XPS measurements of Li, Na, Mg, and Al. Comparisons between the lifetime, phonon, and scattering phase shift values obtained in our XPS measurements with those determined from x-ray absorption spectra will be made in II.

A. Core-hole lifetimes

For core holes with energy less than 2 keV, nonradiative Auger electron emission is the predominant decay mechanism.[26] Two types of Auger decay processes can be defined: those involving higher-lying core electrons, which we refer to as intra-atomic transitions, and those involving either a core and a valence electron or two valence electrons exclusively, which we refer to as interatomic transitions. Intra-atomic transitions predominate in cases where they are energetically allowed.[26] Their probabilities are, by definition, insensitive to chemical environment. Interatomic transitions, on the other hand, while generally weaker on an absolute scale, are the predominant decay mechanisms for certain shallow core holes and clearly depend on the nature of the valence electrons. In other words, for particular core holes the chemical environment of the hole-state atom can affect the lifetime of the hole itself. These considerations have been previously discussed[27] and very dramatic effects of core-hole lifetimes with chemical environment have been recently observed.[28] For the metals Li, Na, Mg, and Al it is, therefore, appropriate to distinguish between those core holes which decay by interatomic, as opposed to intraatomic, transitions and to compare the measured core-hole lifetimes in the metals with those calculated or determined for their atomic counterparts.

Intra-atomic Auger rates are generally calculated from atomic matrix elements using first-order time-dependent perturbation theory.[26] This approach is entirely suitable for the 1s vacancies in metallic Na, Mg, and Al, which decay primarily via KLL transitions. The smaller probabilities for the radiative decay processes, i.e., emission of $K\alpha$ x rays, can also be calculated in a straightforward way. Several authors have calculated the 1s lifetimes in atomic Na, Mg, and Al.[29-31] Their results are compared in Fig. 14 with our measured values in the respective metals. We have included the theoretical[29-31] and experimental[32] values for atomic Ne 1s as well. The monotonic increase of lifetime width with Z is clearly seen. The trend is qualitatively understood as arising from the contraction and consequent increased overlap of the 1s hole with the $n=2$ electrons in this essen-

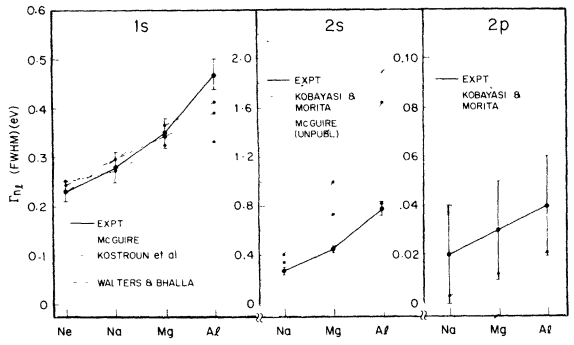

Fig. 14. Comparison of experimental and calculated lifetime widths at FWHM of 1s, 2s, and 2p core holes in Na, Mg, and Al metals. Experimental values from analysis of x-ray photoemission data (this work), except for Al 1s (from Ref. 1) and Ne 1s (from Ref. 32). Theoretical values from Refs. 29, 30, 31, 34, and 35. Note difference in energy scales for different core levels.

tially isoelectronic series. The overlap with the delocalized valence electrons is much smaller. The agreement between theory and experiment is generally very good, although for Al the theoretical values are all somewhat too small.[33]

The calculation of 2s hole lifetimes in Na, Mg, and Al is more difficult. The intra-atomic transitions $L_I L_{II,III} L_{II,III}$ are energetically forbidden so that the only available decay mechanism in the metals are via interatomic Coster-Kronig $L_I L_{II,III} V$ processes. The evaluation of the appropriate transition matrix elements involves an accurate knowledge of the metal valence electron wave functions surrounding the localized core hole. Kobayasi and Morita[34] first applied a diagrammatic many-body scheme for calculating the L_I level widths in these metals by considering the self-energy of a particular core state to be representative of its level width. The results of these authors, along with our experimental values, are shown in Fig. 14. The agreement for Na is satisfactory, but for Mg and Al the calculated width is too large by more than a factor of 2. The 2s levels are short-lived because of the large L_I-$L_{II,III}$ orbital overlap in the Coster-Kronig transitions, and thus the relaxed 2s and 2p wave functions must be quite accurately known. The additional requirement of accurately describing the delocalized valence wave functions and the nature of its exchange with the 2p wave functions in the Auger exchange matrix element makes the calculation of the 2s lifetime unusually difficult by this approach.

McGuire[35] has recently calculated the 2s hole lifetimes in atomic Na, Mg, and Al. His results are also included in Fig. 14. He has shown that the transition probabilities strongly depend on the kinetic energy of the Auger electron, thereby demonstrating the sensitivity of the calculations on the detailed nature of the wave functions involved. The improved agreement of his results with the present measurements in the metals may, however, be fortuitous since the atomic 3s wave functions are not representative of the Bloch states in the conduction band of the metals. Reliable calculations of such transitions in the metals will probably remain elusive.

The 2p hole lifetimes are also difficult to determine for the simple metals because they decay via interatomic $L_{II,III}VV$ transitions. Kobayasi and Morita[34] used their methods to evaluate these lifetimes as well, but were considerably more successful than in the case of the 2s states. Comparison of their results with our measured lifetimes in Fig. 14 shows values too small by about a factor of two, but essentially within our experimental uncertainty.

A 1s vacancy in atomic Li cannot decay nonradiatively since there is only one 2s electron available; even radiative decay is formally dipole forbidden. In metallic Li the interatomic *KVV* decay mechanism is possible because of the valence electrons available in the conduction band. Two approaches have been used to calculate the interatomic Auger rate of Li 1s in metallic Li, an atomic and a many-body scheme. Franceschetti and Dow[36] used an atomic approach in which they assumed the Li conduction electrons surrounding the Li 1s vacancy to be approximated by Li $1s2s^2$. Using relaxed atomic Li 1s orbitals, they obtained a quasiatomic Li 1s lifetime width of 0.040 eV. They then argued that this value should be increased further, at least by the ratio of the Wigner-Seitz to atomic 2s orbital radii, giving a net lifetime width of 0.130 eV. Using a similar scheme Mahan[37] has estimated the 1s level width in Li to be 0.2–0.3 eV. The many-body approach of Kobayasi and Morita[34] was applied to Li by Bergersen, Jena, and McMullen,[38] who calculated the Li 1s lifetime to the lowest diagrammatic order to be approximately 0.008 eV. Those authors pointed out that their result did not include the increased charge density around the 1s vacancy and therefore the true value was expected to be considerably larger than the one they had calculated. Very recently Glick and Hagen[39] extended their approach to include higher-order diagrammatic terms and calculated an increased Li 1s width of 0.0174 eV. Using their methods they also calculated the Na 2p lifetime in Na metal. Comparison of our experimental value of 0.03 ± 0.02 eV for the 1s lifetime width of Li with all the theoretically calculated values shows that only the detailed

many-body formalism by Glick and Hagen produces good agreement.

B. Phonons and other temperature-dependent phenomena

In this section we discuss a variety of effects in XPS spectra of metals whose magnitudes depend on temperature. The most obvious ones are related to electron-phonon coupling, but we will also consider such effects as recoil-phonon broadening and electron binding energies, which are also temperature dependent. Furthermore, the important relation between the magnitude of the phonon-related effects and the lifetime of the hole state will be discussed. Many of the above effects produce a "broadening" of the XPS line shape, so it is important to distinguish them empirically whenever possible. New methods for doing this are presented below. We first summarize a few basic concepts about phonons and hole-state lifetimes which are essential for understanding the discussions that follow.

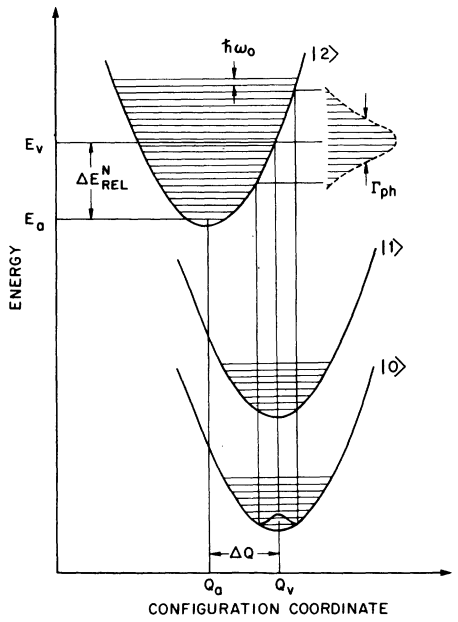

FIG. 15. Configuration coordinate diagram of system with three electronic states and a single vibrational frequency ω_0 assuming the Born-Oppenheimer and harmonic approximations. States $|0\rangle$ and $|1\rangle$ are the ground and excited states of the neutral and photoionized system, respectively. State $|2\rangle$ is the excited state of the ionized system which is reached from the ground state in the photoemission process and which decays to $|1\rangle$. The deformation produced by the core hole is shown by shift ΔQ [Q(vertical)$-$ Q(adiabatic)] in the equilibrium lattice position and by nuclear relaxation energy shift $\Delta E^N_{\rm rel}$. The approximately Gaussian width at FWHM, $\Gamma_{\rm ph}$, of Franck-Condon phonon envelope is also indicated.

Consider the simplest case of an Einstein solid of reduced mass M in which the motion of the atoms or ions is harmonic with frequency ω_0. Although there are many degrees of freedom in a solid, to simplify the discussion it is useful to choose one effective coordinate Q, such as the one directly connecting the hole-state atom to its surrounding neighbors.[7] The initial neutral electronic ground state $|0\rangle$ of the solid is represented by the configuration coordinate diagram shown in Fig. 15. Photoionization of a core electron produces a state $|2\rangle$ whose potential is also harmonic and whose equilibrium position is linearly displaced from $|0\rangle$ by ΔQ, corresponding to a nuclear relaxation (readjustment) energy $\Delta E^N_{\rm rel} = \frac{1}{2} M\omega_0^2(\Delta Q)^2$. All relevant electronic and x-ray transitions are vertical in Q and the Franck-Condon principle applies, i.e., we are in the "sudden approximation" limit (see Sec. IV D for further discussion of the sudden approximation). At some time following photoionization $|2\rangle$ decays into a final, long-lived state $|1\rangle$ which is assumed to be unshifted from $|0\rangle$ as shown in Fig. 15. Thus the lattice is deformed when a hole is in $|2\rangle$, but not when it is in $|1\rangle$. The purpose of introducing $|1\rangle$ is to illustrate the relationship between the lifetime of the core hole in $|2\rangle$ and the degree of phonon broadening of the photoelectron in going from $|0\rangle$ to $|2\rangle$. This has been treated in more detail elsewhere[40] and only the essential arguments are summarized below.

Let us assume that the lifetime of $|2\rangle$ is long, i.e., long with respect to ω_0^{-1}, so that $|2\rangle$ can be treated as the final state. It is possible to think of phonon excitation in two different (but of course equivalent) ways. The first and more common one focuses on the final state $|2\rangle$. Sudden creation of a core hole causes the initial-state wave functions to contract, producing excited eigenstates of the ion. The contracted positive ion couples to the surrounding nuclei and excites phonons. The eigenstates of $|2\rangle$ are thus thought of as being "shaken-up" from $|0\rangle$, and in this language phonons are vibrational analogs of electronic satellites of the final state system. For vibrational transitions in the sudden approximation, the distribution of the closely spaced states is strictly Poisson.[7] In the classical limit, i.e., when the mean number $\bar{n}$ of such states is very large, the distribution becomes Gaussian and the strength of the (relaxed) adiabatic transition is therefore very weak. The FWHM of a Gaussian Franck-Condon envelope at 0° can easily be shown to equal $2(2\ln 2)^{1/2}(\Delta E^N_{\rm rel}\,\hbar\omega_0)^{1/2}$.[7] At finite temperatures the width is multiplied by the statistical Bose-Einstein factor for a thermal ensemble, $[\coth(\hbar\omega_0/2kT)]^{1/2}$.

The second and less common way of thinking about phonon excitation focuses more on the initial

state. The zero-point motion of a harmonic oscillator has a probability distribution that is strictly Gaussian centered around the equilibrium position. Without thinking about the details of the accessible final states for the moment but just assuming that there are enough of them to assume a classical limit, we can imagine suddenly removing an electron from the fluctuating oscillator at different positions so that we essentially sample the complete probability distribution of the initial state. The resulting distribution must therefore be Gaussian. In order to determine its width, we need only consider the displacement and distribution of individual phonon states in $|2\rangle$. The result will, of course, be just that given in the final state picture above.

The importance of considering the fluctuating initial state is seen when the lifetime of $|2\rangle$ is short, i.e., when it is much less than ω_0^{-1}. If the potential wells are arranged as in Fig. 15, we can imagine $|2\rangle$ decaying into $|1\rangle$ so rapidly that no lattice excitations are created because $|0\rangle$ projects directly onto the eigenstates of $|1\rangle$. Nevertheless, in this short-lifetime limit the distribution of photoelectrons excited from $|0\rangle$ to $|2\rangle$ must still be broadened by the fluctuations in $|0\rangle$ to the same extent as in the long-lifetime limit above and for exactly the same reasons. The only difference now is that the individual eigenstates are lifetime broadened so that the resulting photoelectron energy distribution is *simply a convolution* of a Gaussian and Lorentzian. This result is very important because it justifies the data-analysis procedures described in the previous section, i.e., regardless of whether the lifetime and phonon periods are *long* or *short* with respect to one another, the net result will be to produce a Gaussian phonon envelope for sufficiently large $\bar{n}$.

(If the lattice is not excited into higher phonon states in this short lifetime limit, how can the additional energy be carried away by the photoelectron? It is not, of course; an equal and opposite amount of energy is carried away by the emitted decay photon or Auger electron in going from $|2\rangle$ to $|1\rangle$. Coincident detection of the energy distribution for the *sum* of photoelectron-plus-decay species would clearly be a δ function, even though the measurement of the individual distributions themselves are phonon broadened.[40] In a sense, then, it appears that the lattice is "virtually" excited into higher phonon states.)

The intermediate case in which the hole-state lifetime of $|2\rangle$ is *comparable* to the phonon period has been considered by Minnhagen[41] and more recently by Almbladh and Minnhagen.[42] In Minnhagen's original work, he proposed that in this intermediate-lifetime regime there should be an enhanced broadening of the photoemitted electron over and above that described by a simple Gaussian and Lorentzian convolution in either the long- or short-lifetime limits. Although no simple physical picture of the enhancement emerges from the formalisms of his work, it may be understood by imagining the wave functions in $|2\rangle$ becoming slightly out of phase with the wave functions in $|0\rangle$, so that when $|2\rangle$ decays into $|1\rangle$ there is an additional broadening effect because of a few "real" lattice excitations.[40] In such a situation, then, the photoelectron samples not only the fluctuating ground state of the lattice (i.e., the "virtual" excitations), but also some of the "real" excited lattice states as well. Below we shall discuss examples of core holes whose lifetimes are short (e.g., Na 2*s*) and intermediate (e.g., Li 1*s*), and shall consider the importance of the interference effect proposed by Minnhagen. Before doing so, however, it is necessary to outline a few more basic concepts.

In the above discussion, we considered an Einstein lattice because it has only a single lattice frequency ω_0. This model is most appropriate for ionic solids in which ω_0 may be adequately represented by the longitudinal-optical frequency ω_{LO}. Metals, on the other hand, are described by the Debye model in which there is a distribution of frequencies up to the Debye cutoff value, ω_D. The zero-point motion can still be represented by the root-mean-square deviation σ of the atoms from their equilibrium energy (as in the case of an Einstein solid), but now it is less straightforward to picture it simply as in Fig. 15. Furthermore, the statistical weighting factor for the thermal ensemble is somewhat different. It can be expressed by a function due to Overhauser,[43] namely, $[1+(8kT/3\hbar\omega_D)^2]^{1/4}$, where the Debye temperature $\Theta_D = \hbar\omega_D/k$. The two different weighting factors for Einstein and Debye solids are compared in Fig. 16. For the same effective phonon energies $\hbar\omega = 0.03$ eV, the functions are seen to be quite distinct. Alternatively, if the factors are set equal at 300 °K, the corresponding effective phonon frequencies assume the values indicated in the figure. The point to be made here is that only good statistics at several temperatures could distinguish between the functions.

Summarizing the FWHM phonon widths in the large phonon limit due to *electronic* contraction of an atom in a solid at temperature T, we have

(i) Einstein solid:

$$\Gamma_{\rm ph}^{\rm el} = 2(2\ln 2)^{1/2}\sigma_E[\coth(\hbar\omega_0/2kT)]^{1/2}, \quad \omega_0 \approx \omega_{LO}\,; \tag{3}$$

(ii) Debye solid:

$$\Gamma_{\rm ph}^{\rm el} = 2(2\ln 2)^{1/2}\sigma_D[1+(8kT/3\hbar\omega_D)^2]^{1/4}, \quad \omega_D \approx k\Theta_D/\hbar\,.$$

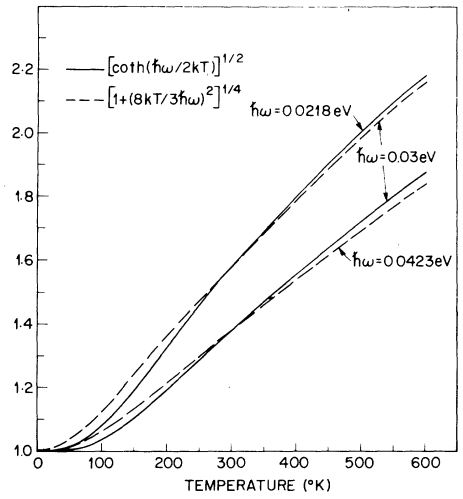

FIG. 16. Comparison of temperature-dependent statistical weighting functions for Einstein (solid line) and Debye (dashed line) thermal ensembles, each with vibrational energies $\hbar\omega = 0.03$ eV. Also shown are the weighting functions of the two models with different vibrational energies produced by requiring they be equal to magnitude at 300 °K. This illustrates importance of measuring phonon widths [see Eq. (3)] over a wide temperature range to determine the true effective vibrational frequency. Debye function taken from Ref. 43.

There is an additional source of phonon excitation that we have not yet considered, namely, the *recoil* energy which the photoejected electron imparts to the ion.[25] Ordinarily the recoil energy is small, but for highly energetic electrons or for low-Z ions it can become quite appreciable. Flynn[25] has recently discussed this effect and has expressed the FWHM Gaussian phonon broadening due to recoil by

$$\Gamma_{\rm ph}^{\rm rec} = \begin{cases} 2(2\ln 2)^{1/2}\left(\dfrac{P^2kT}{M_0}\right)^{1/2} & \text{for } kT > \epsilon_0 \\ 2(2\ln 2)^{1/2}\left(\dfrac{P^2\epsilon_0}{2M_0}\right)^{1/2} & \text{for } kT < \epsilon_0 , \end{cases} \tag{4}$$

where P is the recoil momentum, M_0 the ionic mass, and ϵ_0 the zero-point energy of the solid. P is equal to the photoelectron momentum $[2m_e(\hbar\omega - E_B)]^{1/2}$, where m_e is the electron mass, $\hbar\omega$ the incident photon energy, and E_B the binding energy of the core electron. In the low-temperature limit, one can assume as an upper limit that $\epsilon_0 = \frac{1}{2}\hbar\omega_D$.

The total FWHM Gaussian broadening in an XPS measurement is given by combining the electronic and recoil terms of Eqs. (3) and (4) in quadrature,

$$\Gamma_{\rm ph}^{\rm XPS} = [(\Gamma_{\rm ph}^{\rm el})^2 + (\Gamma_{\rm ph}^{\rm rec})^2]^{1/2} . \tag{5}$$

This is the equation that must be used to interpret the XPS results.

In Table I we have listed the FWHM Gaussian widths of all the XPS data that we have fit by either our least-squares routine or computer-generated comparison procedure. The value of $\Gamma_{\rm ph}^{\rm XPS}$ does not include the instrumental response function. It is worthwhile to also remove the recoil contribution from $\Gamma_{\rm ph}^{\rm XPS}$ in order to make comparisons with theoretical calculations and ultimately with x-ray absorption measurements for which $\Gamma_{\rm ph}^{\rm rec}$ is essentially zero. The Gaussian recoil corrections for photoelectrons emitted with Al $K\alpha$ radiation are readily removed from $\Gamma_{\rm ph}^{\rm XPS}$ using Eqs. (4) and (5), leaving the phonon broadening due to electronic contraction, $\Gamma_{\rm ph}^{\rm el}$.

In Fig. 17, we plot $\Gamma_{\rm ph}^{\rm el}$ values for Li 1s electrons as a function of temperature. For the 90 °K data of Li 1s, the zero-point energy ϵ_0 was approximated by $\frac{1}{2}k\Theta_D$. The error bars include the cumulative uncertainties of the least-squares fitting procedure (negligible) and the instrumental response function, and thus represent the accuracy of the determined widths. For completeness we also include in the plot (shown as open circles) the phonon broadening results of our analysis of x-ray absorption[44] and photoyield[44,45] measurements of the Li K edge. Details of the edge analyses are reported in II. The XPS data have been fit by the temperature-dependent function for Debye solids,

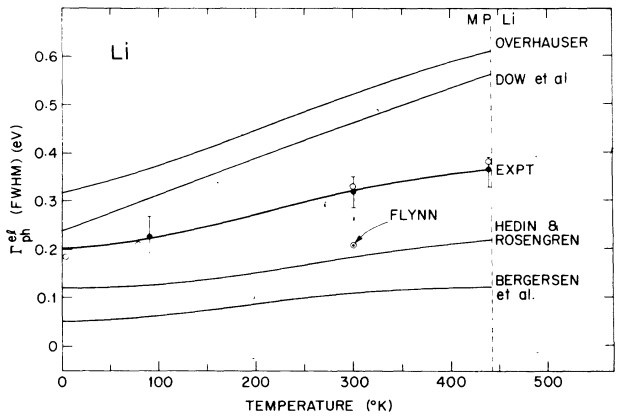

FIG. 17. Comparison between experimental and theoretical temperature dependence and magnitude of electron-phonon broadening $\Gamma_{\rm ph}^{\rm el}$ of Li 1s core hole in Li metal. X-ray photoemission results (filled circles) do not include recoil phonon broadening contribution [see Eq. (5)]. Also shown are electronic phonon broadening results from analysis (Ref. 1) of Li K-x-ray edges (from Refs. 44 and 45). Solid experimental curve is fit to data assuming Debye solid, Eq. (3). Calculated values for generating theoretical curves were taken from Refs. 25, 43, 47, and 50–53. Note that none of the theories shown can account for the experimental data.

Eq. (3), shown as a solid line. The phonon cut-off energy $\hbar\omega_D$ in Eq. (3) was a free parameter in the fit and was found to be 0.029 ± 0.004 eV for $\Gamma_{sp} = 0.25 \pm 0.02$ eV. Significantly, this is smaller than the phonon cut-off energy of 0.035 eV deduced from the Debye temperature of Li.[46] The extrapolated phonon width at $T = 0°$, $\Gamma_{ph}(0°)$, using the empirical cut-off energy of 0.029 ± 0.004 eV is 0.20 ± 0.03 eV.

The empirical evaluation of $\hbar\omega_D$ and $\Gamma_{ph}(0°)$ is believed to be the first of its kind. The values will be seen below to be important in attempting to explain the long-standing discrepancies between calculated phonon widths in Li and those observed. Phonon broadening in Li is particularly important in the understanding of the Li K edge.[17] We shall, however, defer this issue to paper II. The emphasis here will be on the general phenomenon of phonon broadening in XPS line shapes of Li and the other simple metals.

We compare our XPS phonon widths for Li with various calculations in Fig. 17. Overhauser's deformation potential model,[43,47] which was first applied to Li by McAlister,[48] clearly gives values too large even when the Fermi energy of 3.32 eV is used[49] (McAlister used the free electron value of 4.70 eV). The "indirect" phonon mechanism of Dow, Robinson, and Carver[50,51] results in values greatly in excess of those measured. Bergersen, Jena, and McMullen[38] argued persuasively that the "indirect" coupling model is really equivalent to the conventional hole-phonon broadening scheme. Using a rather sophisticated approach, however, Bergersen, McMullen, and Carbotte[52] were also unable to reproduce the magnitude of phonon broadening in Li. Very recently, Hedin and Rosengren[53] have carefully considered the effects of phonon broadening in Li and have obtained considerably better success. Another recent effort to calculate Γ_{ph}^{el} for Li by Flynn[25] gave a value of 0.210 eV at 300 °K compared with the observed width of 0.32 eV at that temperature. Unfortunately, the temperature dependence of the phonon broadening contribution using his semiempirical model was not presented. A general comparison of the present experimental results with those from all the various theories[25,43,49,52,53] spanning almost seven years is encouraging but certainly not wholly gratifying.

Minnhagen's[41] proposal of interference between the lifetime decay and phonon broadening mechanisms offers a possible explanation for the discrepancies. Recall that this model suggests that when the core-hole lifetime and phonon period are comparable, there should be an enhanced broadening of the photoemission spectrum over that predicted by a simple convolution of lifetime and phonon contributions. Comparison of the Li 1s lifetime of 0.03 ± 0.02 eV with a typical phonon period determined from the Debye temperature of $k\Theta_D = 0.035$ eV[46] shows them to meet the necessary condition of being comparable in magnitude.

The effects of the interference between phonon generation and hole-state decay can be tested in three ways. The first and most obvious, of course, is to compare the calculated phonon width in the absence of interference with experiment. This has already been done above and the disagreement no doubt was the initial motivation for the formulation of Minnhagen's[41] theory. However, the lack of agreement by itself is not conclusive because the measured widths contain both temperature-dependent and -independent terms, either or both of which could produce discrepancies. A second, more stringent test is to compare the terms individually and this has been accomplished in the above analysis. We have seen that the empirical cut-off energy $\hbar\omega_D$ is smaller than that predicted in the absence of an interference related phenomenon, thereby suggesting its existence. The third and final test involves the measured cut-off energy and the empirical zero-point (i.e., temperature *in*dependent) phonon width $\Gamma_{ph}(0°)$. Knowing both $\Gamma_{ph}(0°)$ and $\hbar\omega_D$, the Stokes-shift energy $2E_0$ between absorption and emission edges can be calculated from Debye theory. This is given by $E_0 = (4/3)\sigma_D^2/\hbar\omega_D$,[53] where σ_D from Eq. (3) is $\Gamma_{ph}(0°)/2(2\ln 2)^{1/2}$. Using the empirical values of σ_D and $\hbar\omega_D$, one predicts $2E_0 = 0.66 \pm 0.12$ eV.[54] The observed Stokes-shift energy between Li K edges is no greater than 0.2 eV,[45,55] again in line with the predictions of an interference effect. Thus, we have three results, namely, $\Gamma_{ph}^{el}(T)$, $\hbar\omega_D$, and E_0, which are consistent with an interference-related phenomenon in Li. The phonon broadening for Li can be argued to be larger because, from our discussions above, creation of a 1s core hole on the time scale of its lifetime produces both real and "virtual" lattice excitations.

It would be interesting to make similar comparisons of our measured phonon width for Na, Mg, and Al with calculations to assess the general importance or correctness of a phonon-lifetime interference effect, but detailed XPS temperature studies have not been extended to these systems. Only for Mg have we made two separate measurements at 90 and 300 °K. In II, we have also analyzed the $L_{II,III}$ absorption edges of these metals, measured at 77 °K,[56] from which the phonon widths have been obtained. The details of the analysis are discussed in II. We present the results in Fig. 18, shown as open circles, along with our XPS phonon widths at room temperature deduced from the 2p and 2s data, shown as filled circles. The XPS values have been corrected for recoil

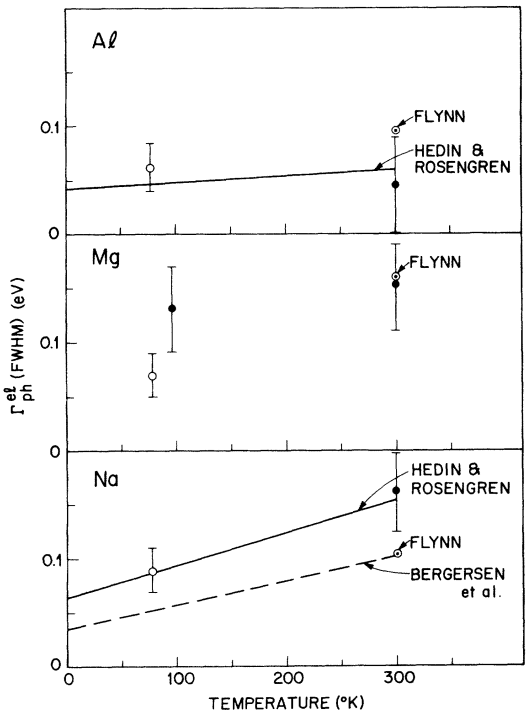

FIG. 18. Comparison between experimental and theoretical electronic phonon broadening Γ_{ph}^{el} of $2p$ and $2s$ core holes in Na, Mg, and Al metals. X-ray photoemission results (filled circles) do not include recoil phonon broadening contribution, see Eq. (5). Also shown are electronic phonon broadening results from analysis (Ref. 1) of $L_{2,3}$ x-ray absorption edges (from Ref. 44). Note that as opposed to Li (see Fig. 19), good agreement is obtained between experiment and theory (from Refs. 25, 52, and 53).

effects using Eqs. (4) and (5) and the assumptions described above for Li. The error bars are relatively large because of the smaller absolute magnitudes of Γ_{ph}^{el}. On general grounds Γ_{ph}^{el} is understood to be smaller than was the case for Li because, among other reasons, the atoms are heavier and removal of a core electron has a smaller fractional perturbation on the other core electrons. The particular trends of the phonon widths from metal to metal is less clear since the effective phonon frequencies and nuclear relaxation energies themselves do not follow a simple pattern.

Comparison of the phonon broadening widths with various theories for Na, Mg, and Al is included in Fig. 18. Overhauser's theory[43] has been omitted because of its large overestimation of the phonon broadening in Li. No temperature-dependent theory is available for Mg. A general inspection of the agreement between theory and experiment for Al and Na shows it to be good. Thus, as opposed to Li, an interference-related broadening does *not* appear to be present in these metals. For Al, the absence of such an effect can be understood because the phonon broadening is itself so small. Hedin and Rosengren calculate $\bar{n} = 0.6$ for Al and experimentally (see Sec. III and Table I) we find virtually no electron-phonon broadening in the Al $2p$ spectrum. Sodium, on the other hand, is clearly phonon broadened; Hedin and Rosengren calculate $\bar{n} \approx 11$. While it may be argued that it is difficult to obtain very accurate measurements of the broadening in Na because of its small magnitude relative to the resolution of the present instrument, the precision (if not the accuracy) of the Na results gains credibility from the nearly identical value observed for the broader, shorter-lived Na $2s$ level. The Mg $2p$ and $2s$ data show similar results as in Na. The Mg broadening is also comparable for the $2p$ and $2s$ states. Approximate empirical phonon cutoff energies determined for Na and Mg are in moderate agreement with $\hbar\omega_D$ determined from the respective Debye temperatures. Furthermore, Stokes-shift energies calculated from the empirical $\hbar\omega_D$'s and extrapolated Γ_{ph} (0°) values do not suggest the existence of a significant interference effect as was found in Li. Therefore, based on the (admittedly meager) data for Na and Mg, it appears experimentally that either the interference effect is sufficiently small in these metals so as to go unobserved, or that the enhanced broadening in Li is due to some other cause. Theoretically, Almbladh and Minnhagen[42] have very recently reconsidered the enhancement effect and find that Minnhagen's original work[41] relating the complex part of the electron-phonon coupling constant with the lifetime width seems to be an oversimplification. Furthermore, it is conceivable that the harmonic approximation may be inappropriate for Li and that the enhanced broadening arises simply from anharmonic lattice distortions. Therefore, it appears that at present no reliable theoretical estimate exists of the *magnitude* of *an* interference effect (should one be present) for comparison with our experimental results.

With regard to the subject of electron-phonon coupling in XPS, we briefly mention another temperature-dependent broadening mechanism discussed first by Ferrel[57] and more recently expanded upon by Almbladh and Minnhagen.[58] This involves not the core hole-phonon coupling, but rather the conduction electron-phonon coupling. As expected, it is very small. In both limits of large and small core hole lifetime and hole-phonon couplings relative to kT, the additional FWHM broadenings amount to < 0.1 eV. This is extremely difficult to observe when convoluted with the larger spectrometer, lifetime, and phonon contributions.

Another interesting question in the above discussion is whether our assumption of a Gaussian phonon distribution is valid in the analysis of the Li 1s linewidths. The criterion for assuming the strong coupling limit is that the coupling strength or mean number of phonons $\bar{n}$ be sufficiently large. The onset of "sufficiently" has been studied in detail by Keil,[59] among others, and his results indicate that for $\bar{n} \geq 5$ the distribution is indeed essentially Gaussian (only at $\bar{n} = \infty$ is it strictly Gaussian). We can calculate what $\bar{n}$ is quite easily. For Einstein solids it is simply $\sigma_E^2/\hbar\omega_0^2$, and for Debye solids it is given by $2\sigma_D^2/\hbar\omega_D^2$ (the factor of 2 comes in because a mean frequency, not the upper Debye cut-off frequency, is required). Using the empirical values of σ_D and $\hbar\omega_D$ for Li we get $\bar{n} \sim 16$, clearly large enough to support the assumption of a Gaussian phonon distribution.

Finally, we turn our attention to the temperature dependence of the Li 1s binding energy, which was observed to increase with increasing temperature. Although the total binding *shifts* (as opposed to broadenings) are small over the entire temperature range of 90–440 °K, it is nevertheless apparent even in the raw data, see Fig. 7. The energy shifts from one temperature to another were determined after each spectrum was fit with the least-squares procedure, and thus does not represent the shifts incurred by convoluting the DS line shape with the instrumental contributions. Based on the analysis below, we identify the shifts as due to a combination of thermal-expansion and temperature-dependent polarization energy. This observation is believed to be the first of its kind in the photoemission spectrum from a metal.

The most obvious source of a temperature effect on electron binding energies in a metal is from lattice thermal expansion. This is a first-order correction in the energy expression of an electron in a solid and arises from the anharmonic dilation of the lattice. Other corrections such as Debye-Waller and Fan (self-energy) effects are second-order in the electron-phonon interaction and are expected to be negligible. It is straightforward to estimate the thermal-expansion effect on the core-level binding energy E_B. The differential volume change of an electron gas is just $dV/V = -\frac{3}{2} dE_F/E_F$. With respect to a fixed E_B which is insensitive to such volume changes, E_F decreases with increasing T. It is not solely E_F which decreases, however, it is the entire width of the conduction band. A more suitable parameter to gauge the dilation of the band is the average Fermi energy $\bar{E}_F = \frac{3}{5} E_F$.[60] Now in an XPS experiment involving a metal, E_B is generally referred to the Fermi level, which is fixed. Therefore, in such a situation E_B becomes the temperature-dependent variable and is related to the change in E_F by $E_{B_2}(T_2) - E_{B_1}(T_1) \equiv \Delta E_B^{\text{th}} = -\bar{E}_F(T_2) + \bar{E}_F(T_1) \equiv \Delta \bar{E}_F$. Assuming the lattice expansion to be linear over the temperature range $\Delta T = T_2 - T_1$ ($T_2 > T_1$), we simply have the binding energy shift due to thermal expansion,

$$\Delta E_B^{\text{th}} \sim -2\alpha_L \bar{E}_F \Delta T \,, \tag{6}$$

where α_L is the linear thermal expansion coefficient equal to $(1/3V)dV/dT$. Equation (6) states the intuitive notion that as the temperature increases, the core electrons become less tightly bound because of the weaker attractions in the expanded lattice.

The trend of binding energy with temperature is, however, *opposite* to what is observed: E_B of Li 1s increases with increasing temperature. The reason for this is that the polarization energy of the screening conduction electrons is reduced as the lattice volume increases. This heretofore neglected effect can be readily evaluated by expressing the polarization energy in terms of an effective screening length λ_{sc}; classically this is just the image screening or polarization energy $E_{\text{pol}} = e^2/2\lambda_{sc}$. The change in effective screening volume with temperature then goes as

$$\frac{dV}{V} = 3\alpha_L dT = \frac{3d\lambda_{sc}}{\lambda_{sc}} = -\frac{3dE_{\text{pol}}}{E_{\text{pol}}} \,. \tag{7}$$

Since the binding energy increases with decreasing E_{pol}, i.e., $\Delta E_B = E_{B_2}^{\text{pol}}(T_2) - E_{B_1}(T_1) \equiv -\Delta E_{\text{pol}}$, we have the simple expression for the total binding energy shift (i.e., the sum of initial-state thermal and final-state polarization binding energy shifts),

$$\Delta E_B^{\text{tot}} = \Delta E_B^{\text{th}} + \Delta E_B^{\text{pol}} = \alpha_L \Delta T(-2\bar{E}_F + E_{\text{pol}}) \,. \tag{8}$$

The only calculated value in Eq. (8) is E_{pol} and this has been determined elsewhere to range between 6.6 eV[61] and 7.4 eV.[62] Using the Li Fermi energy of 3.3 eV,[49] and the linear expansion coefficient of 4.5×10^{-5} K^{-1},[63] we calculate total binding energy shifts which range between 0.025–0.32 eV and 0.016–0.22 eV for the temperature ranges of 90–300 °K and 300–440 °K, respectively. These compare favorably with the observed values of 0.029 and 0.018 eV. It is also gratifying that the present model predicts a negligible binding energy shift for Mg, ≤ 0.008 eV, because no detectable shift was found in the present experiments, see Fig. 13.

C. Applicability of the Doniach-Šunjić line shape to XPS data

We have shown above how we can extract core hole lifetimes and phonon broadening factors from measured XPS core level line shapes using the Doniach-Šunjić (DS) function,[6] Eq. (2). In the next section we will show using Eqs. (1), (2), and Friedel's sum rule, how we can also extract scattering

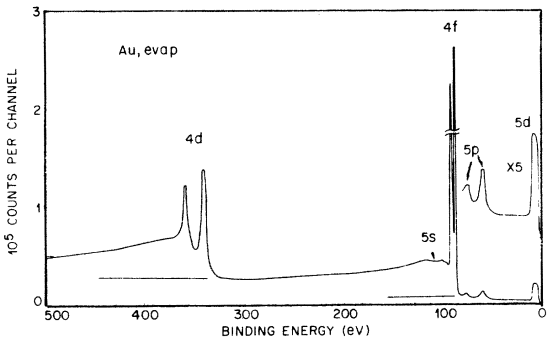

FIG. 19. Wide-energy (low-resolution) x-ray photoemission spectrum of Au 4*f* and 4*d* electrons from evaporated gold. Note that energy loss tails of the two levels are *comparable* but that peak heights are very different (the Au 4*f* peaks actually run off the figure). It *appears* that the peaks and tails are inseparable (compare with Fig. 20).

phase shifts from the XPS data. In view of the detailed information being obtained from these measurements, we must clearly justify our use of Eq. (2) before placing confidence in the parameters obtained. In the previous section, we have shown that it is valid to represent the effects of phonon and lifetime broadening by a convolution of Gaussian and Lorentzian line shapes. Here we shall address the question of whether Eq. (2) correctly represents the e-h pair response by asking (i) over what energy interval from the XPS peak the DS function is valid, and (ii) whether there are any other contributions to the measured XPS spectrum that preclude the direct application of the DS function to the data. For simplicity of presentation, we consider the second question first.

In Sec. I, we alluded to the fact that the theoretical formulation of the DS function for XPS[6] preceded the observation of the phenomenon[8,9] by almost three years. This seems particularly puzzling in view of the distinctive line shape shown in Fig. 1. Technological limitations do not satisfactorily account for the lapse, since even before high-vacuum and high-energy resolution were achieved, the XPS asymmetry could be clearly discerned in the data. The real reason undoubtedly lies in the fact that extrinsic inelastic energy losses were believed responsible for the observed effects. This is not surprising because the elastically scattered photoelectrons comprise only a very small fraction of the total electron flux emerging from a solid as a consequence of the large differences in x-ray penetration and electron escape depths (microns versus angstroms). In fact, a typical wide-energy low-resolution photoemission spectrum makes it appear that the inelastic tail and elastic peak are inseparable.

In Fig. 19, we show such a spectrum of the Au 4*f* and Au 4*d* photoelectrons. The inelastic tails of the two levels are comparable because the photoelectric cross sections are comparable. Displaying the separate spectra on a finer resolution in Fig. 20, however, creates the apparent paradox that the Au 4*f* loss tail is now smaller than that for the Au 4*d* electrons. This, however, is merely due to the fact that the 4*f* levels are narrower (longer lived) and so their amplitude is larger in order to conserve peak area. It only *appears* in Fig. 20 that the total elastic/inelastic area ratios are different for the two levels because the energy scales have been changed and heights normalized. Part of the conceptual difficulty arises from the limited resolution in a wide energy scan; the true amplitude of the Au 4*f* peaks would run off the top of Fig. 19.

From Fig. 20, it is clear that it would be difficult, if not impossible, to separate the inelastic from the elastic contributions in the Au 4*d* spectrum because the lines are so broad. Only for the narrow Au 4*f* levels is there the possibility of making this separation *in practice*. The next question, then, is whether it is possible *in principle* to separate the inelastic from elastic components of even an infinitely narrow core level spectrum.

Recall that there are two predominant modes of energy loss for electrons in a free-electron metal,

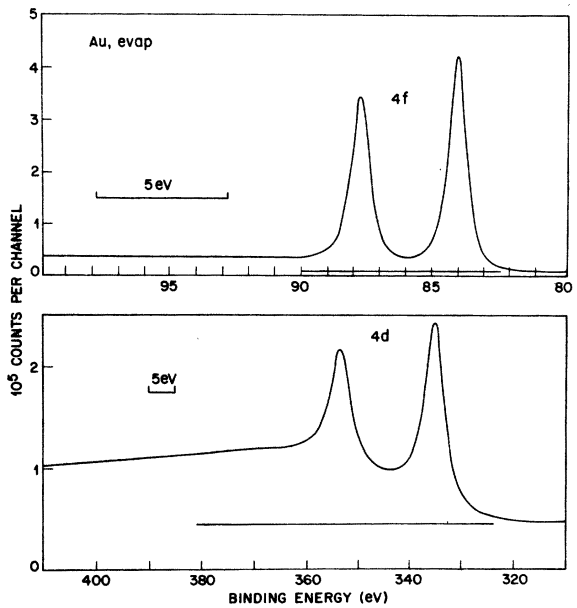

FIG. 20. Narrow-energy (high-resolution) x-ray photoemission spectra of Au 4*f* and 4*d* electrons from evaporated gold. Note that because of *difference in energy scales* it *appears* that energy loss tails of Au 4*f* peaks are *smaller* than those of Au 4*d* peaks (compare with Fig. 19).

namely, excitation of plasmons and electron-hole pairs. (There are, of course, in addition to these processes the usual atomic-like "shake-up" transitions.) Moreover, there are two distinct physical ways of producing these excitations. One is during the transport of the photoelectron to the surface and into the vacuum; this is referred to as an extrinsic process. The other is during the production of excited eigenstates of the many-electron systems upon the sudden creation of the core hole; this is an intrinsic property of the core hole spectrum. Distinguishing between extrinsic and intrinsic plasmons is a procedure we need not discuss for our present purposes. This follows because plasmons occur at discrete energies which are generally well removed in energy from the main XPS peak (see Sec. II). On the other hand, e-h pairs are produced in the XPS tail close to the main peak. Distinguishing between extrinsic and intrinsic e-h's is made by the following theoretical and experimental arguments.

The cross sections for producing e-h pairs as a function of electron energy have recently been calculated by Tung *et al.*,[64] and their results indicate that even at kinetic energies of only a few tens of eV, the cross sections are vanishingly small. Photoelectrons from core levels excited by 1.5 keV radiation have kinetic energies of several hundred eV and are, therefore, expected to have a negligible effect on the intrinsic e-h pair spectrum of XPS line shapes near the main peak. Direct empirical evidence to support this expectation has already been given in Sec. II. Sodium 2s and 2p electrons have kinetic energies of >1400 eV in our experiments, whereas the kinetic energies of 1s electrons are of the order of 400 eV. The electron escape depths of 1s electrons is conservatively estimated to be about a factor of 2 smaller than that of the 2s and 2p electrons.[65] One manifestation of the smaller 1s electron escape depth of Na is directly observable in Fig. 10, where the trace oxidized impurity and surface plasmon intensities are both larger relative to the main peak than in the 2s spectrum. *In spite of the differences in escape depths, however, the same value of α is determined for all the core levels in a given metal.* This evidence strongly demonstrates the negligible contribution of extrinsic e-h pairs to the XPS line shape in these systems over the stated narrow energy ranges.

As we have seen above for the Au 4d electrons, however, there *can* be interference from other discrete excitations. The core level width must definitely be narrower than the nearest allowable excitation. For free-electron metals this energy is usually the surface plasmon energy, but for other metals (such as Au) interband transitions of lower energy are possible. (In Au, for example, an energy loss is observed at 4 eV which is well outside the region of analysis in the narrow Au 4f spectrum, but well inside that of the Au 4d spectrum.)

There are two lessons to be learned from all this. First, it is indeed possible to analyze the intrinsic e-h pair contribution to the XPS line shape without interference from extrinsic features, *provided the analysis is performed on core levels whose lifetime widths are narrow relative to the first accessible excitation.* Second, since the XPS line shape does contain a tail of e-h pairs that is *intrinsic* to its shape, it is incorrect to subtract any "background" from the raw data in the hopes of making an inherently asymmetric line shape symmetric.

What other factors must be considered in the analysis of XPS line shapes? There appear to be five, three of which have already been discussed in detail, namely, phonons, lifetime, and instrumental broadening. The other two are mentioned here for completeness: they are surface impurities and surface structure, i.e., non-bulk-like behavior of the metal. They are sometimes cited as being of concern because the "surface-sensitivity" of the XPS technique throws doubt on the ability to attribute the results of analysis to the bulk. We have, however, explicitly shown above for the 1s and 2p electrons of Na that small amounts of trace surface impurity have little effect on the analysis. For large amounts of surface impurity closer in energy to the substrate metal peak this would, of course, no longer be true, but this situation is usually academic in systems prepared under ultra-high-vacuum conditions. With regard to the possibility that measurements are so surface-sensitive as not to sample the bulk of the material, the above results for Na 1s and 2s core levels serve to discount that extreme suggestion. (Surface-sensitivity can, of course, be enhanced by detecting electrons emitted at near grazing angles.) In the absence of any known evidence to the contrary, therefore, the XPS measurements presented here appear to be representative of the bulk.

Having established that there are no spurious or inherently artifactual contributions to the XPS line shape, we now consider over what energy range from the main peak the DS function should remain valid. To our knowledge this question has not been thoroughly examined from first principles, but several workers have treated the problem in a variety of ways. The $1/\epsilon^{1-\alpha}$ dependence was initially derived only in the limit of small excitations, and depends upon the joint density of e-h pair states being proportional to ϵ.[4,5] The functional form away from the peak requires evaluation of the terms in the power series describing the interac-

TABLE II. Singularity index for Mg 2s spectra as a function of energy from the main peak.

Energy region from main peak (eV)	α [a]	Γ_{2s} [a] (eV)
3	0.129±0.007	0.465±0.035
1	0.132±0.012	0.462±0.044
0.5	0.115±0.024	0.459±0.042

[a] Support plane error limits are shown.

tion potential of the collective excitations. Mahan[37] has considered the first four terms and finds that the sum of the series corresponds to the result obtained by replacing sinδ by δ in the first term. Minnhagen[66] has recently shown that starting with a simple dielectric response function for the conduction electrons, the Mahan formalism[37] leads to a result similar to that of DS which adequately describes the data up to the first plasmon energy (he ignored surface plasmons). The effects of structure in the density of states has also been considered[67] ignoring both the plasmon response and any energy dependence of the matrix elements. It was found that for completely-free-electron metals, the DS function describes the data to within 3% up to energies of $\frac{1}{2}E_F$ from the peak. For more complex joint density of states additional modifications in the theory are required, but ones that are entirely tractable.

In the present work, we have attempted to study empirically the range of validity of the DS function by varying the energy region from the peak in which the data are analyzed. The Mg 2s spectrum was chosen for study because the statistics are reasonably high, it is only a single peak (i.e., there is no spin-orbit splitting), the Mg surface is atomically clean, and there is no interference from the surface plasmon structure. The energy ranges over which the data were fit varied from 3 to 0.5 eV, or $0.43E_F$ to $0.071E_F$. The α values determined from the least-squares routine are listed in Table II. Note that in spite of the larger limits of uncertainty as the number of data points decreases, the values of α remain essentially unchanged.

None of the above-mentioned theoretical or experimental efforts are by themselves definitive, but taken in concert all point to the same conclusion: that the DS function should provide a good description up to energies of the order of half the width of the occupied band, i.e., *greater* than the interval used in our analyses. At present there does not seem to be any reason to doubt the applicability of the DS function to data as we have used it in this work.

D. Singularity indices

In this section, we discuss the singularity indices determined from the XPS data of Li, Na, Mg, and Al. The emphasis will be on establishing a physical correspondence between their magnitudes and the conduction electron screening of core holes. The implications of the magnitudes of the scattering phase shift values on the $L_{II,III}$ and K x-ray edge problem will be treated in detail in II.

It is well known that a core hole in a metal is screened by the conduction electrons in such a way as to lower the total energy of the system. Let us start with this simple notion and see what can be learned from the present measurements of α. The simplest point of view is that the core hole attracts one conduction electron which screens the unit extra positive charge. It is more fruitful to consider the scattering of the conduction electrons by the attractive potential of the hole. This introduces the concept of scattering phase shifts, δ_l, which obey the Friedel sum rule, and can be thought to represent partial screening charges, q_l, which add up to the amount of charge being screened. From this point of view the screening charge is simply due to the change of the trajectories of conduction electrons as they pass an attractive potential. For the case of unit charge, the Friedel sum rule becomes

$$Z = \frac{2}{\pi}\sum_{l=0}^{\infty}(2l+1)\delta_l = \sum_l q_l = 1 . \tag{9}$$

The singularity index is usually expressed in terms of δ_l's, see Eq. (1). Since *e-h* pair production is a manifestation of the screening process and α is a measure of the *e-h* pairs, it follows from Eq. (9) that α can also be expressed in terms of the partial screening charges, i.e.,

$$\alpha = \frac{2}{\pi^2}\sum_l (2l+1)\delta_l^2 = \tfrac{1}{2}\sum_l \frac{q_l^2}{2l+1} . \tag{10}$$

The square of the charge enters from the fact that it is the amount of charge of the electrons and of the holes which determines the strength of the *e-h* pair interaction. In fact, in a spinless one-band metal with constant density of states, it can be shown[5] that α is proportional to the square of the density of states which enters through the calculation of the joint density of *e-h* pair states. This solution, however, does not satisfy the Friedel sum rule. In real metals the degeneracy factors of spin and orbital angular momenta plus the details of the band structure itself must be taken into account. As shown elsewhere[67] the band-structure effects in simple metals have negligible influence on the line shape, so that our α measurements in

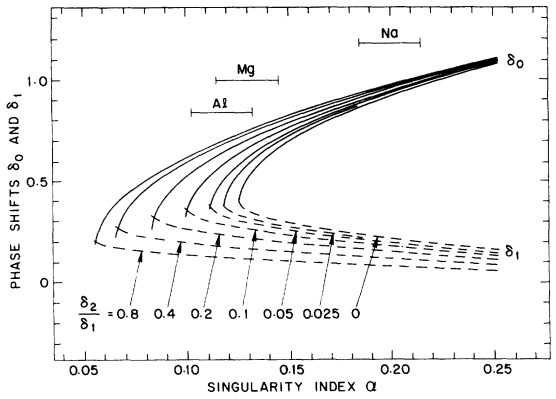

FIG. 21. Friedel phase shifts as a function of singularity index in a three-phase-shift analysis using the Friedel sum rule with $Z=1$. Solid and dot-dashed curves correspond to positive s and p phase shifts, respectively, which have been terminated at points of comparable magnitude. Families of curves for fixed d/p phase-shift ratios are indicated. The experimental range of singularity indices for Na, Mg, and Al measured in this work are shown by horizontal bars.

Li, Na, Mg, and Al provide a rather direct evaluation of the screening charge in these systems. With this in mind, our analysis is straightforward.

The Friedel sum rule, Eq. (9), and the definition of α, Eq. (10), yield an upper limit of $\alpha_{max}=0.5$ for the case when there is only screening from electrons with s symmetry, i.e., $\delta_0=\frac{1}{2}\pi$ and $\delta_l=0$ for $l\geq 1$. The minimum value of α is obtained when all the phase shifts are equal. This is given by

$$\alpha_{min}=1/m\ , \tag{11}$$

where

$$m=\sum_{l=0}^{l_{max}} 2(2l+1)\ .$$

Thus, for s- and p-type screening ($l_{max}=1$), $\alpha_{min}=\frac{1}{8}$; for screening involving electrons of s, p, and d symmetry, $\alpha_{min}=\frac{1}{18}$, and so on. As the fractional contribution of δ_0 decreases, so does α.

The α values of Na, Mg, and Al from Table I are 0.20, 0.13, and 0.12, respectively. The monotonic but nonuniform trend is clear. The conduction band of sodium is essentially half-filled with electrons of s symmetry. The nature of the screening charge in Na metal has been previously described[8] to be s-like in the comparison of the Na $2p$ optical transition energy in Na atom (corresponding to Na $2p^63s^1 \rightarrow$ Na $2p^53s^2$) with the Na $2p$ binding energy in Na metal [corresponding to $(\text{Na } 2p^6)_{CB} \rightarrow (\text{Na } 2p^5)_{CB'} + e^-$; CB and CB′ are the initial ground and final relaxed conduction bands, respectively]. The near equivalence of the two energies is direct evidence that the relaxed conduction band in Na with a core hole is essentially represented by the $3s^2$ configuration in atomic Na, i.e., the screening electron occupies what can be thought of as an s-like Friedel bound state, where in this case the impurity in Na metal is a Na^+ ion. In magnesium, where the s band is more nearly filled, the Friedel state is largely p-like; in Al the conduction band is even more p-like. The sharp drop in s character (or conversely the increase in p character) of the screening charge in going from Na to Mg is clearly larger than that in going from Mg to Al. The qualitative trend of α values, which we have seen above to be a sensitive measure of δ_0, quite naturally reflects that break.

It is desirable to quantify the relative amounts of partial screening charges for a given α. If we make the simplifying but reasonable assumption (as we shall see) that screening electrons of no greater than d symmetry are important in the free s-p electron metals studied here, we may plot δ_0 and δ_1 vs α for different fixed values of δ_2/δ_1. These are shown in Fig. 21. The curves are terminated where δ_0 and δ_1 are of comparable magnitude. Also, we show only the regions where the phase shifts are positive since this corresponds to the attractive interaction between the screening charges and the hole. The horizontal bars correspond to our measurements. From this figure, we see that the range of phase-shift values allowable from our measurements of α is large for Mg and Al, but is reasonably well confined for Na. Unfortunately, this situation cannot be avoided because the number of unknowns exceeds the number of equations. Comparison with various calculations in Table III,[37,62,66,68-70] however, is gratifying and considerably reduces the spread for the case of Na, Mg, and Al. Only Mahan's results[37] are in disagreement with our measurements because of an overestimation of the δ_2 contribution in the scattering. The disagreement with experiment between Girvin and Hopfield's[68] calculations

TABLE III. Comparison of experimental and theoretical singularity indices.

	Li	Na	Mg	Al
Experiment	0.23	0.20	0.13	0.12
Theory				
Ref. 69	0.20	0.19		
Ref. 20	0.18	0.20		
Ref. 37	0.22	0.14	0.10	0.09
Ref. 66	0.24	0.21	0.13	0.11
Ref. 62	0.16	0.20		0.13
Ref. 68	0.16	0.12		

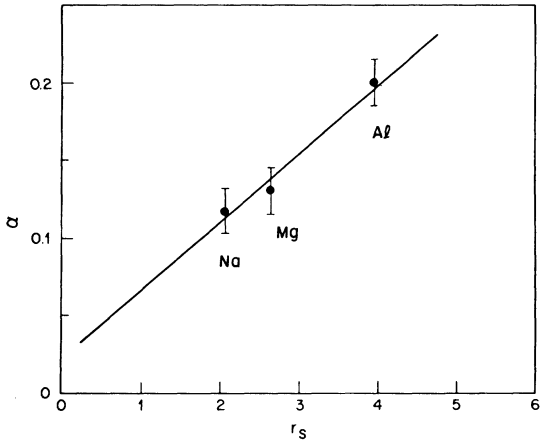

FIG. 22. Singularity index for Na, Mg, and Al as a function of electron radius parameter. The nonzero α value at $r_s = 0$ is not significant since α is not expected to be strictly proportional to r_s.

for Na and the other results for Li will be discussed below. For Na, Mg, and Al, however, inspection of all the individual phase shifts calculated from the various theories[37,62,66,69,70] places an upper limit of $\delta_2/\delta_1 \sim 0.2-0.3$. Thus our assumption of higher-order scattering phase shifts being unimportant in these simple metals is entirely warranted.

Since α is a measure of the conduction-electron screening it is tempting to correlate α with the electron radius parameter, r_s, which is a measure of the electron density. This is done in Fig. 22, from which the strong correlation is apparent. Dow and Sonntag[71] suggested a similar comparison but included Li in their analysis as well. This is clearly incorrect. Li is in a different period from the other metals and the core-core interactions between atoms whose cores are isoelectronic with He and Ne are, of course, considerably distinct. r_s is thus not to be taken as an absolute measure of free-electron density, but rather only a relative one amongst atoms that are in all other respects similar. It is also for this reason that no physical significance should be attached to the nonzero value for α at an r_s of zero.

The distinction between Li and Na, Mg, and Al arising from their being in different periods is believed to have still another effect in the interpretation of α. In our discussions above, we have assumed that the isoelectronic Ne cores of Na, Mg, and Al have no effect on the screening conduction electrons. Girvin and Hopfield[68] have argued that in Li this assumption breaks down because the exchange coupling between the Li 1*s* and conduction-band electrons is non-negligible due to the strong overlap at the nucleus. The spins of the hole of the screening electrons are therefore important; in effect spin-up and spin-down electrons appear separately in the sum rule. This has the consequence that α, which just measures the square of the screening charges, will not be directly comparable with the α values of the third-row elements in which the exchange mixing is expected to be considerably weaker. The fact that the weighted sum of the squares of the spin-up and spin-down phase shifts does not add up to the measured singularity index in Na serves to demonstrate the difficulty of such a calculation in a metal in which the exchange is not even expected to be important.

We conclude this section by briefly discussing the validity of the sudden approximation, which was tacitly assumed in the interpretation of the phonon and *e-h* pair distributions observed in this work. The sudden approximation assumes that the core hole potential is created so rapidly that the eigenstates of the neutral atom project into the excited eigenstates of the ion with probabilities determined solely by the energies of the ion eigenstates involved according to simple time-dependent perturbation theory. The criterion for assuming the sudden approximation is that sufficient energy is available to excite enough higher-lying states such that additional energy would make a negligible contribution to the total relaxation of the ion. In the case of 1*s* photoemission from atomic neon, for example, the probability for exciting the 2*p* electron into the continuum (a "shake-off" transition) has been shown to remain essentially constant for 1*s* photoelectron kinetic energies in excess of ~250 eV.[72] This energy corresponds to roughly five times the threshold energy of 48 eV necessary to eject the 2*p* electron from a neon atom with a 1*s* hole. It can, in effect, be thought of as the "onset" of the sudden approximation for Ne 1*s* photoemission.

It would be desirable to determine empirically the "onset" of the sudden approximation for other excitations such as plasmons, phonons, and *e-h* pairs. This could be achieved, in principle, using synchrotron radiation. In practice, however, such experiments for *e-h* pairs and phonons are extremely difficult to interpret in these terms because the energies of these excitation processes are so small. For low photoelectron kinetic energies, structure in the unfilled conduction band, autoionization processes, and the energy dependence of the photoelectric cross sections are all sure to complicate the detailed analysis of line shapes. Recent synchrotron studies of the shape of vibrational envelopes in diatomic molecules provide clear evidence of this fact.[73] Insofar as

determining the onset of the sudden limit for plasmons is concerned, the problem is even less clear in spite of the fact that these excitations have sufficiently large energies to avoid the problems of additional structure in the final state. Some calculations maintain[74] that the sudden limit for plasmons is not reached even for photoelectron kinetic energies of a thousand eV,[75] because of an interference effect between the outgoing electron and the polarizable electrons around the core hole. Firm experimental proof of this effect at these energies remains to be demonstrated.

In the absence of determining the onset of the energy regimes at which the sudden approximation is applicable to the e-h pair and phonon spectra, we can nevertheless be confident that in the present XPS experiments involving electrons with kinetic energies >100 eV the sudden approximation is indeed valid. For vibrational excitations there is ample evidence which shows that in the XPS energy regime[76] the vertical transition energy (see Fig. 17) is observed rather than the adiabatic transition energy seen in photoemission spectra measured in the ultraviolet energy regime.[77] For e-h pair excitations recent calculations[78] of the energy dependence of its spectrum give clear evidence that only for very low photoelectron kinetic energies, typically <10 eV, can an energy distribution distinguishable from the $1/\epsilon^{1-\alpha}$ behavior be observed. Finally, the extremely good agreement of the line shapes assuming the sudden approximation with the XPS data presented here serve to confirm the validity of its assumption.

V. SUMMARY

Analysis of core level photoemission spectra from Li, Na, Mg, and Al has led to a detailed understanding of the three physical processes which affect the intrinsic line shape. These include the core hole lifetime, the many-body response of the conduction electrons, and the phonon and recoil excitation of the lattice. In order to extract this information, careful account was taken of the effects of the instrumental resolution function and of contributions from plasmon excitation and surface contamination. Evidence is presented which directly shows that extrinsic electron-hole pairs do not make a significant contribution to the line shape in the vicinity of the peak, and that the line shape described by Doniach and Šunjić provides a good representation of the screening process to within $\frac{1}{2}E_F$ from the peak in these metals.

Quantitative results for the three fundamental parameters were obtained for all core levels accessible with Al $K\alpha$ radiation. Comparison with the relevant theories allows critical choices to be made in cases where the range of calculated values is large. Temperature dependent phonon broadening was found in both Li and Mg, with indications that an interference effect may be responsible for the enhanced broadening observed in Li. Temperature-dependent core-level binding energies in Li were also observed and explained by simple theory.

---

[1] P. H. Citrin, G. K. Wertheim, and M. Schlüter (unpublished).

[2] G. D. Mahan, Phys. Rev. 163, 612 (1967).

[3] P. Nozières and C. T. DeDominicis, Phys. Rev. 178, 1097 (1969).

[4] P. W. Anderson, Phys. Rev. Lett. 18, 1049 (1967); Phys. Rev. 164, 352 (1968).

[5] J. J. Hopfield, Commun. Solid State Phys. 2, 40 (1969).

[6] S. Doniach and M. Šunjić, J. Phys. C 3, 285 (1970).

[7] See, for example, M. H. L. Pryce, in *Phonons in Perfect Lattices with Point Imperfections*, edited by R. W. H. Stevenson (Oliver and Boyd, Edinburgh, Scotland, 1966), p. 403; J. J. Markham, Rev. Mod. Phys. 31, 956 (1959).

[8] P. H. Citrin, Phys. Rev. B 8, 5545 (1973).

[9] S. Hüfner, G. K. Wertheim, D. N. E. Buchanan, and K. W. West, Phys. Lett. 46A, 420 (1974).

[10] P. H. Citrin, P. Eisenberger, and D. R. Hamann, Phys. Rev. Lett. 33, 965 (1974).

[11] Y. Baer, G. Busch, and P. Cohn, Rev. Sci. Instrum. 46, 466 (1975).

[12] During the course of this work, detailed analyses of all Li, Na, Mg, and Al line shapes and also those of Au and Ag showed that the width and form of the AEI spectrometer function varied somewhat between measurements of different metals. This is not surprising because the response function depends critically on the alignment of the sample, the electrostatic focusing lenses, and the crystal monochromator, none of which can be considered strictly invariant. For the Al 2p measurements, the function was an extremely narrow and symmetric Gaussian, for Na it was still symmetric but somewhat broader, for Li it was about the same width as for Na but was very slightly skewed, and for Mg it was rather skewed and broader still. Only for the Mg measurements was it necessary to include the effects of a skewed Gaussian instrumental function in the data analysis (see Ref. 13).

[13] G. K. Wertheim, J. Electron. Spectrosc. Relat. Phenom. 6, 239 (1975).

[14] G. K. Wertheim and S. Hüfner, J. Inorg. Nucl. Chem. 38, 1701 (1976).

[15] S. Hüfner and G. K. Wertheim, Phys. Rev. B 11, 678 (1975).

[16] P. H. Citrin, G. K. Wertheim, and Y. Baer, Phys. Rev. Lett. 35, 885 (1975).

[17] Y. Baer, P. H. Citrin, and G. K. Wertheim, Phys. Rev. Lett. 37, 49 (1976).

[18] D. W. Marquardt, J. Soc. Indust. Appl. Math. 11, 431

(1963).
[19]P. H. Citrin, G. K. Wertheim, and Y. Baer (unpublished).
[20]L. Ley, F. R. McFeely, S. P. Kowalczyk, J. G. Jenkin, and D. A. Shirley, Phys. Rev. B 11, 600 (1975).
[21]T. Kloos, Z. Phys. 265, 225 (1973).
[22]C. Kunz, Z. Phys. 196, 311 (1966).
[23]H. Fellenzer, Z. Phys. 165, 419 (1961).
[24]See references cited in Ref. 21.
[25]C. P. Flynn, Phys. Rev. Lett. 37, 1445 (1975).
[26]W. Bambynek, B. Crasemann, R. W. Fink, H.-U. Freund, H. Mark, C. D. Swift, R. E. Price, and P. V. Rao, Rev. Mod. Phys. 44, 716 (1972).
[27]P. H. Citrin, Phys. Rev. Lett. 31, 1164 (1973); J. Electron. Spectrosc. Relat. Phenom. 5, 273 (1974).
[28]J.-N. Chazalviel, M. Campagna, G. K. Wertheim, P. H. Schmidt, and Y. Yafet, Phys. Rev. Lett. 37, 919 (1976).
[29]E. J. McGuire, Phys. Rev. A 2, 273 (1970).
[30]V. D. Kostroun, M. H. Chen, and B. Crasemann, Phys. Rev. A 3, 533 (1971).
[31]D. L. Walters and C. P. Bhalla, Phys. Rev. A 4, 2164 (1971).
[32]U. Gelius, J. Electron. Spectrosc. Relat. Phenom. 5, 985 (1974).
[33]The Al 1*s* lifetime was determined in Ref. 1 from data of H. Neddermeyer, Phys. Rev. B 13, 2411 (1976), and agrees with Neddermeyer's analysis.
[34]T. Kobayasi and A. Morita, J. Phys. Soc. Jpn. 28, 457 (1970).
[35]E. J. McGuire (unpublished).
[36]D. R. Franceschetti and J. D. Dow, J. Phys. F 4, L151 (1974).
[37]G. D. Mahan, Phys. Rev. B 11, 4814 (1975).
[38]B. Bergersen, P. Jena, and T. McMullen, J. Phys. F 4, L219 (1974).
[39]A. J. Glick and A. L. Hagen, Phys. Rev. B 15, 1950 (1977).
[40]P. H. Citrin and D. R. Hamann, Phys. Rev. B 15, 2923 (1977).
[41]P. Minnhagen, J. Phys. F 6, 1789 (1976).
[42]C.-O. Almbladh and P. Minnhagen (unpublished).
[43]A. W. Overhauser, quoted in A. J. McAlister, Phys. Rev. 186, 595 (1969).
[44]C. Kunz, H. Petersen, and D. W. Lynch, Phys. Rev. Lett. 33, 1556 (1974).
[45]H. Petersen, Phys. Rev. Lett. 35, 1363 (1975).
[46]N. F. Mott and H. Jones, *The Theory of the Properties of Metals and Alloys* (Dover, New York, 1958), p. 14.
[47]In calculating Γ_{ph}^{el} with Overhauser's model, Ref. 43, we used Debye temperatures from Ref. 46 and acoustic velocities from H. C. Nash and C. S. Smith, J. Phys. Chem. Solids 9, 113 (1959).
[48]A. J. McAlister, quoted in Ref. 43.
[49]M. J. G. Lee, Phys. Rev. 178, 953 (1969).
[50]J. D. Dow, J. E. Robinson, and T. R. Carver, Phys. Rev. Lett. 31, 759 (1973).
[51]In calculating the temperature-dependent phonon broadening contribution from the model of Ref. 50, we used the rms lattice data from H. G. Smith, G. Dolling, R. M. Nicklow, P. R. Vijayaraghavan, and M. K. Wilkinson, in *Proceedings of the Fourth LAEA Symposium on Neutron Inelastic Scattering, Copenhagen, Denmark, 1968* (International Atomic Energy Agency, Vienna, Austria, 1968), p. 149.
[52]B. Bergersen, T. McMullen, and J. P. Carbotte, Can. J. Phys. 49, 3155 (1971).
[53]L. Hedin and A. Rosengren, J. Phys. F 7, 1339 (1977).
[54]Note that the uncertainties in the predicted E_0 are correlated with $\Gamma_{ph}(0°)$ and $\hbar\omega_D$ because as $\Gamma_{ph}(0°)$ increases, so does $\hbar\omega_D$, and vice versa.
[55]T. A. Calcott and E. T. Arakawa, Phys. Rev. Lett. 38, 442 (1977).
[56]C. Kunz, R. Haensel, G. Keitel, P. Schreiber, and B. Sonntag, *Electronic Density of States*, edited by L. H. Bennett, U. S. Natl. Bur. Stand. Spec. Publ. No. 323 (U.S. G.P.O., Washington, D. C., 1971), p. 275.
[57]R. A. Ferrell, Phys. Rev. 186, 399 (1969).
[58]C.-O. Almbladh and P. Minnhagen (unpublished).
[59]T. H. Keil, Phys. Rev. 140, A601 (1965).
[60]We thank M. Schlüter for discussions on this point.
[61]L. Hedin and S. Lundqvist, in *Solid State Physics*, edited by F. Seitz, D. Turnbull, and H. Ehrenreich (Academic, New York, 1969), Vol. 23, p. 159.
[62]C.-O. Almbladh and U. von Barth, Phys. Rev. B 13, 3307 (1976).
[63]W. B. Pearson, *A Handbook of Lattice Spacings and Structures of Metals and Alloys* (Pergamon, New York, 1958).
[64]C. J. Tung, R. H. Ritchie, J. C. Ashley, and V. E. Anderson, Oak Ridge National Laboratory Report No. 5188, 1976 (unpublished).
[65]See, for example, C. J. Powell, Surf. Sci. 44, 29 (1974).
[66]P. Minnhagen, Phys. Lett. 56A, 327 (1976).
[67]G. K. Wertheim and L. R. Walker, J. Phys. F 6, 2297 (1976).
[68]S. M. Girvin and J. J. Hopfield, Phys. Rev. Lett. 34, 1320 (1975).
[69]G. A. Ausman, Jr. and A. J. Glick, Phys. Rev. 183, 687 (1969).
[70]P. Longe, Phys. Rev. B 8, 2572 (1973).
[71]J. D. Dow and B. F. Sonntag, Phys. Rev. Lett. 31, 1461 (1973).
[72]T. A. Carlson and M. O. Krause, Phys. Rev. 140, A1057 (1965).
[73]E. W. Plummer, T. Gustuffson, D. E. Eastman, and W. Gudat (unpublished).
[74]J. J. Chang and D. C. Langreth, Phys. Rev. B 5, 3512 (1972); 8, 4638 (1973).
[75]J. W. Gadzuk, J. Electron. Spectrosc. Relat. Phenom. (to be published).
[76]For example, see K. Siegbahn, C. Nordling, G. Johansson, J. Hedman, P. F. Hedén, K. Hamrin, U. Gelius, T. Bergmark, L. O. Werne, R. Manne, and Y. Baer, *ESCA Applied to Free Molecules* (North-Holland, Amsterdam, 1969).
[77]For example, see D. W. Turner, C. Baker, A. D. Baker, and C. R. Brundle, *Molecular Photoelectron Spectroscopy* (Wiley-Interscience, London, 1970).
[78]J. W. Gadzuk and M. Šunjić, Phys. Rev. B 12, 524 (1975).